

ABSTRACT

GOVIND, BALA. Dynamic In-Vitro Assessment of Microbubble-Mediated Dual-Frequency High Intensity Focused Ultrasound (HIFU) Induced Thrombolysis (Under the direction of Dr. Yun Jing).

Optimizing the use of high intensity focused ultrasound (HIFU) for recanalization of occluded blood vessels is an actively researched area. This yields an alternative therapy to the use of thrombolytic drugs in the treatment of ischemic stroke. HIFU treatment, used in conjunction with microbubbles in the fluid stream, serves to augment the dissipation of the blood clot. In this study, using an *in vitro* approach, a flow system is implemented to simulate the dynamic dispersion of blood clots using single-frequency focused ultrasound (SFFU) and dual-frequency focused ultrasound (DFFU). The effects of permutations of acoustic power and driving frequency (SFFU vs. DFFU) on the rate of disintegration and site-specific lytic action are quantified using digital image processing under the influence of fluid akin to that in a blood vessel, for a specific microbubble concentration. It is found that dual-frequency excitation, in general, produces a faster rate of clot dissipation in comparison with single-frequency excitation and this observation is corroborated by cavitation signal detection. Observations indicate that accelerated thrombolysis may be realized by the inertial cavitation threshold of DFFU being lower than that of SFFU. Further, thrombolytic effect with variance in microbubble concentration is studied for a fixed acoustic power. Efficacy of DFFU is not found to vary appreciably with an increase in microbubble concentration from 10^8 MBs/ml to 10^9 MBs/ml, possibly due to acoustic shadowing induced at increased concentrations. The analysis is extended to study the effects of substituting MBs for nanodroplets and investigating their influence on thrombolysis by SFFU and DFFU. It was found that onset of acoustic droplet vaporization before inertial cavitation yields inconsistent trends and, in comparison with MBs, engenders little advantage when used in conjunction with DFFU.

© Copyright 2018 by Bala Govind

All Rights Reserved

Dynamic In-Vitro Assessment of Microbubble-Mediated Dual-Frequency High Intensity
Focused Ultrasound (HIFU) Induced Thrombolysis

by
Bala Govind

A thesis submitted to the Graduate Faculty of
North Carolina State University
in partial fulfillment of the
requirements for the degree of
Master of Science

Mechanical Engineering

Raleigh, North Carolina

2018

APPROVED BY:

Dr. Yun Jing
Committee Chair

Dr. Marie Muller

Dr. Xiaoning Jiang

BIOGRAPHY

Bal Govind began his Master of Science degree at North Carolina State University in the Fall of 2016. He was subsequently involved in thrombolysis research at Dr. Yun Jing's Acoustics and Ultrasonics Laboratory and completed work comprising this thesis in the Summer of 2018. Prior to joining NCSU, he worked in the capacity of a contract engineer in Bangalore, India after obtaining his Bachelor's degree in Mechanical Engineering at Vellore Institute of Technology (India) in 2014. He is inter-disciplinary and currently focuses on electromechanical systems with applications in the energy and aerospace industries.

ACKNOWLEDGEMENTS

I would like to acknowledge the contribution of several students and faculty members at the Department of Mechanical and Aerospace Engineering at North Carolina State University:

- Dr. Yun Jing and Dr. Dingjie Suo for giving me the opportunity to contribute to the lab's ongoing project on thrombolysis. Their guidance and attention to detail are greatly appreciated.
- Dr. Jinwook Kim, Huaiyu Wu and other members of Dr. Xiaoning Jiang's lab for provision of peripheral instrumentation and microbubble and nanodroplet vials for our experiments.
- Mr. Andrew Anthony for his timely assistance over the Summer of 2017.
- Every other member of our lab and Dr. Marie Muller's lab for their support and patience with our work.
- Dr. Ashley Brown, Department of Biomedical Engineering, for her advice on practical aspects of the thrombolysis experiment.

I sincerely hope that our work over the past year helps deepen the collective insight into the mechanisms and factors affecting the application of High Intensity Focused Ultrasound in thrombolysis.

TABLE OF CONTENTS

LIST OF TABLES	vi
LIST OF FIGURES	vii
CHAPTER 1: Introduction to High Intensity Focused Ultrasound induced thrombolysis.....	1
1.1 - Motivation for HIFU-mediated clinical treatment	1
1.2 - Theoretical and experimental factors in MB mediated HIFU induced thrombolysis	4
1.2.1 - Numerical factors considered in simulation of microbubble dynamics	4
1.2.2 - Experimental considerations in HIFU-mediated thrombolysis	8
CHAPTER 2: Design of the HIFU-induced thrombolysis experiment	12
2.1 - Clot preparation	12
2.2 - Microbubble solution preparation	12
2.3 - Experimental apparatus and data acquisition	13
2.4 - Flow system.....	14
2.5 - Alternate motorized arrangement for mounting and focusing the HIFU transducer....	15
CHAPTER 3 - Experimental quantification of clot dispersal rate and indentation efficacy	19
CHAPTER 4 - Results and discussion.....	22
4.1 - Experimental results of MB-mediated thrombolysis using a flow model.....	22
4.2 - An extended analysis for Nanodroplet-mediated thrombolysis using a flow model....	27
CHAPTER 5 - Conclusions and scope of future work	33
REFERENCES	35
APPENDICES	42
APPENDIX A - MATLAB® code for image processing of HIFU–induced thrombolysis and control of Arduino® Braccio arm	43
APPENDIX B - Representative images used in post-processing of site-specific clot indentation size for DFFU (1.45 MHz +1.5 MHz) and SFFU (1.5 MHz)	61

LIST OF TABLES

Table 1.	(a) Length of motorized-arm segments	18
	(b) Range of angular operation for base, shoulder, elbow and wrist motors	18

LIST OF FIGURES

Figure 1	Normalized waveforms of single, dual, and triple-frequency excitations. Reprinted from [43].	6
Figure 2	Inertial cavitation thresholds of single-, dual-, and triple-frequency excitations. (a) the criterion of $R_{max} = 2R_0$ and (b) the criterion of $\frac{dR}{dt} = -c$. Reprinted from [43].	7
Figure 3	Inertial cavitation thresholds of dual-frequency excitations with different power allocations, in blood using (a) the criterion of $R_{max} = 2R_0$ and (b) the criterion of $\frac{dR}{dt} = -c$. Reprinted from [43].	7
Figure 4	Normalized average clot width vs. time for clots exposed to ultrasound enhanced thrombolysis at different duty cycles (Meunier et al. 2007)	9
Figure 5	Thrombolytic efficacy, as determined by percent mass loss, for plasma alone, 3.15 $\mu\text{g}/\text{mL}$ rt-PA, and rt-PA, Definity + ultrasound treatments (Sutton et al. 2013)	10
Figure 6	Sequential bright-field microscopic images of a microbubble adjacent to a thrombus during ultrasound delivery (1 MHz, 1.5 MPa) recorded at 5 Mfps. (Chen et al. 2014)	11
Figure 7	In vitro experimental setup to examine microbubble-mediated HIFU-induced thrombolysis	15
Figure 8	A second arrangement consisting of a motorized arm, HIFU transducer, clot holder and flow system in the MB-mediated thrombolysis experiment	16
Figure 9	Articulated, Arduino-controlled arm employed for better focusing (a) Relative position of motors M2 and M3 used in the shortened configuration. (b) 2-D workspace of the end-effector (transducer T2) in the YZ-plane.	17
Figure 10	Image processing of (a) an untreated clot and (b) a clot subjected to MB-mediated HIFU (1.45 MHz + 1.5 MHz)	20
Figure 11	Image processing and estimation of efficacy of microbubble-mediated HIFU treatment for individual indentations along the length of the clot for a representative case of DFFU treatment.	21
Figure 12	Time-transient dissipation of blood clot when subjected to microbubble-mediated (at 109 MBs/ml) SFFU at 1.5 MHz and DFFU of 1.45 MHz + 1.5 MHz for PNPs of (a) 2.5 MPa, (b) 3.0 MPa, (c) 3.5 MPa, (d) 4.0 MPa and (e) 4.5 MPa.	24

Figure 13	Comparison of (a) indentation size as a percentage of initial clot, for varying PNPs for MB-mediated (109 MBs/ml) SFFU (1.5 MHz) and DFFU and (b) overall rate of dissipation during each permutation of the experiment.....	25
Figure 14	Cavitation signals for (a) SFFU and (b) DFFU for various PNP amplitudes at a microbubble concentration of 10^9 MBs/ml.....	25
Figure 15	Time-transient dissipation of blood clot subjected to microbubble-mediated SFFU and DFFU at a PNP amplitude of 3.5 MPa for microbubble concentrations of (a) 0 MBs/ml, (b) 10^8 MBs/ml and (c) 10^9 MBs/ml.....	26
Figure 16	Comparison of (a) indentation size as a percentage of initial clot, with variance in microbubble concentrations for SFFU and DFFU excitation and (b) overall rate of dissipation for each permutation of the experiment at a PNP amplitude of 3.5 MPa	27
Figure 17	Time-transient dissipation of blood clot subjected to DFFU, with and without NDs for PNPs of (a) 2.5 MPa, (b) 3.0 MPa, (c) 3.5 MPa, (d) 4.0 MPa and (e) 4.5 MPa.....	30
Figure 18	Time-transient dissipation of blood clot subjected to SFFU (1.5 MHz), with and without NDs for PNPs of (a) 2.5 MPa, (b) 3.0 MPa, (c) 3.5 MPa, (d) 4.0 MPa and (e) 4.5 MPa.....	31

CHAPTER 1

Introduction to High Intensity Focused Ultrasound induced thrombolysis

1.1 Motivation for High Intensity Focused Ultrasound (HIFU)-mediated clinical treatment

High Intensity Focused Ultrasound (HIFU) is a precise and non-invasive technique used to selectively and locally produce viscous heating and/ or acoustic cavitation in the interior of the body [1]. Currently, HIFU is being investigated for applications in sonothrombolysis [2], histotripsy [3], drug delivery [4], neurosurgery [5] and the thermal ablation of tumors [6] located in various tissues, including kidney, brain, uterine fibroids, bone and liver. Focused ultrasound imaging [7,8] is also being coupled with Magnetic Resonance Imaging (MRI) [9] in clinical monitoring techniques. However, the therapeutic efficiency of HIFU treatment would need to be optimized to realize its practical application in surgical intervention.

Thrombi in brain block cerebral blood vessels and limit the blood supply to brain tissue, causing ischemic stroke [10-12]. The Food and Drug Administration (FDA) currently limits its approval for treatment of acute ischemic stroke to intravenous injection of tissue plasminogen activator (tPA) [13]. This approach, however, has shortcomings in that the patient would need treatment within 4 to 5 hours of the stroke's onset [14] and that the treatment could take several hours to complete [15]. Also, tPA could induce intracerebral hemorrhage and may not always lead to complete recanalization [16]. The use of high intensity focused ultrasound (HIFU) as an effective thrombolysis method has been reported in vitro [17,18], ex vivo [19] and in vivo [20,21].

There are several advantages to the use of HIFU. Firstly, it may be implemented non-invasively and does not require the injection of tPA and therefore could eliminate its side effects [22]. Secondly, the treatment time has been reported to be 1-10 minutes long in vitro, which is

considerably faster than the conventional approach with tPA when dealing with the same amount of clot [23]. Thirdly, the procedure could be guided by a real-time cavitation imaging system for monitoring and target-specific action [24-26].

However, the interposition of the skull poses serious problems to HIFU treatment of ischemic stroke. A MHz frequency is desired due to its finer spatial resolution compared to kHz frequency ultrasound, which is crucial to reducing damage to the vessel and surrounding tissue [27]. Unfortunately, human skulls cause strong absorption due to their porous structure [28,29], especially when the frequency is in the MHz range. This could lead to insufficient acoustic energy at the focus and could make effective disintegration of the embedded clot challenging.

The main mechanism for HIFU-based thrombolysis is inertial cavitation [30,31]. The effects elicited by inertial cavitation, e.g., micro-jetting, streaming, and local heating, can break clot structure and may, therefore, induce thrombolysis [32,33]. In this framework, it would be extremely useful to enhance the inertial cavitation effect to enhance HIFU-based thrombolysis efficiency. Ultrasound contrast agents (UCAs) such as microbubbles (MBs) have been reported to be able to considerably lower the power needed for initiating inertial cavitation without apparent side effects [34-36]. Kajiyama et al. showed a much faster temperature rise in the focal zone of the transducer with the existence of microbubbles [37]. Chung et al. noted an enhancement of the necrosis area in rabbit liver ablation with UCAs compare with HIFU alone [38]. Chen et al. reported a significantly shortened treatment time for the uterine fibroids using SonoVue [39] microbubbles.

However, the power required for HIFU therapy can still be high, even with the addition of UCAs. More efficient methods should be developed to further reduce the acoustic power. Previous studies

indicate that the thrombolysis efficiency, as a percentage of the clot weight, of dual-frequency focused ultrasound (DFFU) is higher than that of single-frequency focused ultrasound (SFFU) [40] [41] in a static model (with or without UCAs). To shed light on the mechanism of DFFU thrombolysis, numerical analysis employing bubble dynamics models [42-43] showed that the cavitation threshold of DFFU is lower than that of SFFU in both fluid and tissue. Zhang and Li [44] demonstrated that the acoustic scattering cross section of a gas bubble under dual frequency acoustic excitation is much larger than that of single frequency excitation. Tataka and Pandit suggested a better energy efficiency of dual frequency in generation of cavitation activity and also pointed out that dual frequency could minimize the formation of standing waves [45].

In this thesis, a simple in vitro approach is implemented to quantify the time-transient dissipation of bovine blood clots. Using a flow system, the dynamic dispersion of the clot using SFFU and DFFU is first compared, with the addition of MBs. Compared to previous studies using a static model, this study provides more temporal information on the thrombolysis efficiency, a more precise control of MBs feeding and the effect of the flow is taken into account which could have impact on cavitation. Also quantified are the effects of varying combinations of peak negative pressure (PNP), i.e., acoustic power, and MB concentration on the rate of disintegration using digital image processing. Further, this method is used to determine efficacy of treatment per site of sonication in an attempt to infer the optimal acoustic energy necessary for DFFU-induced inertial cavitation for a specific MB concentration. Additionally, analysis at this energy and for varied MB concentration yields insight into experimental considerations of using larger microbubble population in a simulated blood vessel. The procedure is then extended to study the effects of nanodroplets and their efficacy in thrombolysis by SFFU and DFFU.

1.2 Theoretical and experimental factors in MB-mediated HIFU induced thrombolysis

1.2.1 Numerical factors considered in simulation of microbubble dynamics

Fast Fourier Transform (FFT) and bubble-response response curves are used to explain the nonlinear bubble dynamics under DFFU and SFFU. The power spectrum and the response curve under DFFU show unique features, known as ‘combination resonances’ and ‘simultaneous resonances’. These resonance frequencies can be expressed by a linear combination of component frequencies. The amplitudes of combination resonances were found to increase with the increase of the pressure amplitude of the sound wave [50]. For a bubble of small equilibrium radius, the amplitudes of combination resonances are suppressed and the thresholds of subharmonics and ultraharmonics are found to be enhanced.

From the waveform of DFFU excitation, it can be inferred that the increased peak negative pressure, in comparison to SFFU, diminishes the cavitation threshold and increases the number of bubbles (nuclei). Furthermore, dual-frequency excitation has less acoustic absorption than the single-frequency mode at the same power because of reduced waveform distortion. Further analysis of the thresholds indicates that these nonlinear mechanisms produce a low-frequency component at the difference frequency $f = f_2 - f_1$ and peaks at frequencies of $nf_1 \pm mf_2$ (where n and m are integers). The multi-frequency excitation facilitates the faster onset of inertial cavitation and enables a reduction in cavitation threshold.

Numerous assumptions are typically made in numerical simulations of free microbubble expansion in a fluid. For example, while employing Gilmore-Akuliches equation in [51], it was assumed that the fluid is homogeneous and isotropic. Secondly, the air bubble was assumed to remain spherical and initially at rest so that bubble dynamics can be calculated in a one-dimensional space. Thirdly,

gas inside the bubble was considered ideally adiabatic ($\gamma=1.4$) and there was no gas or vapor exchange between the gas and the surrounding medium. However, it is claimed that such an omission is not critical because the inertial cavities are not likely to survive more than one or two cycles of excitation. It has been shown that the adiabatic assumption underestimated the maximum bubble radius while the isothermal assumption overestimated it. It was found that although multiple-frequency excitations were able to enhance the temperature elevation in the tissue ablation because of the enhanced inertial cavitation, the temperature elevation in the pulsed ultrasound application, such as sonothrombolysis, is insignificant. Theoretically, the Keller-Miksis equations and Van der Waal's equation with chemical kinetics indicate that the impact of the consideration of reactions heats is dependent of the frequency and the acoustic amplitude of the ultrasonic wave. Further, the introduction of reactions heats has an effect of reducing the minimum radius attained at the end of the collapsing phase of the microbubble, regardless of the frequency and the acoustic amplitude of the ultrasonic wave. Also, the maximum temperature reached at the same point of the oscillation cycle was found to decrease with a ratio that is proportional to the acoustic pressure and inversely proportional to the wave frequency. Further, reactions in either the forward or backward sense are endothermic in character and the product radicals are quantified in percentages like % OH, % H and % O.

Our previous work [43] on prediction of inertial cavitation of microbubbles subjected to multi-frequency ultrasound excitation showed that DFFU will, in general, result in lower cavitation threshold than SFFU. That is, the requisite power for thrombolysis would potentially be reduced if DFFU is employed. However, an accurate simulation cannot be performed without considering the nonlinear distortion of the input acoustic waveform due to the behavior of wave propagation in the fluid medium. Nevertheless, in a qualitative sense, trends obtained from this and several

other models [60,61] have similarities. The investigation showed that DFFU could perform better than SFFU in both fluid and soft tissue. Also, it offers explanations to why DFFU has greater effect with the increase in shear modulus of the surrounding medium. This serves to validate, in part, the experimental observations discussed in the following chapters.

Interestingly, inclusion of a low-frequency component was shown to drastically reduce the threshold and this nuance bears fruit for microbubbles of larger radii. In some cases, it was predicted that the combination of DFFU frequency components could be less effective than SFFU when the component frequencies are multiples of one another. For brevity, a few caveats and observations derived from this numerical modelling are summarized here, using a modified Keller-Miksis model [60]. As in the forthcoming thrombolysis experiment, a comparative analysis is made between acoustic signals of equal power amplitude as shown in Fig. 1, over a standard radius range of $1 \mu m$ to $10 \mu m$ [60-62].

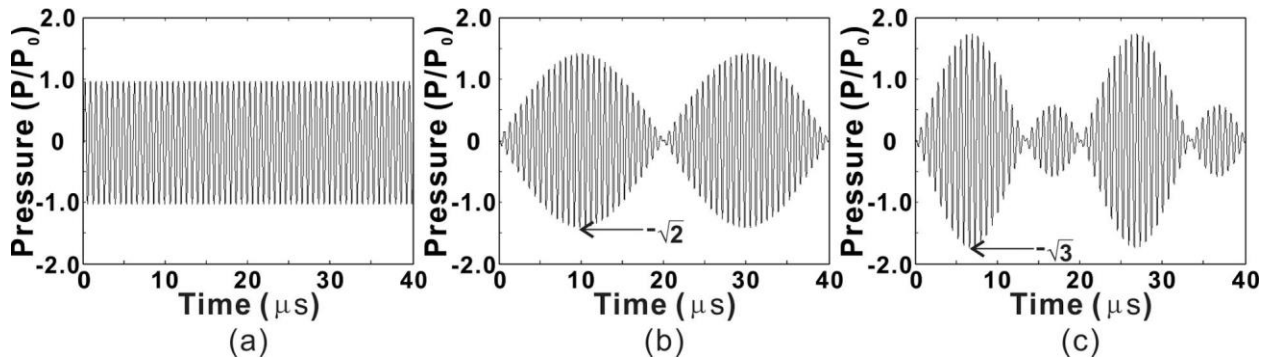


Figure 1. Normalized waveforms of single, dual, and triple-frequency excitations. Reprinted from [43].

The investigation considered two criteria, $R_{max} = 2R_0$ and a bubble-wall velocity of $\frac{dR}{dt} = c$ for the onset of inertial cavitation [60,61]. Figs. 2 (a) and (b) show the calculated inertial cavitation pressure threshold for single-frequency, dual-frequency, and triple-frequency excitation, using both criteria. Observably, the criterion of $\frac{dR}{dt} = c$ is shown to yield higher thresholds. Further, the

minimum cavitation pressure threshold occurs around $2 \mu\text{m}$ where the natural frequency of the microbubble equals the driving frequency. This would imply that the power needed to initiate inertial cavitation continuously decreases with the increase in the number of frequency components.

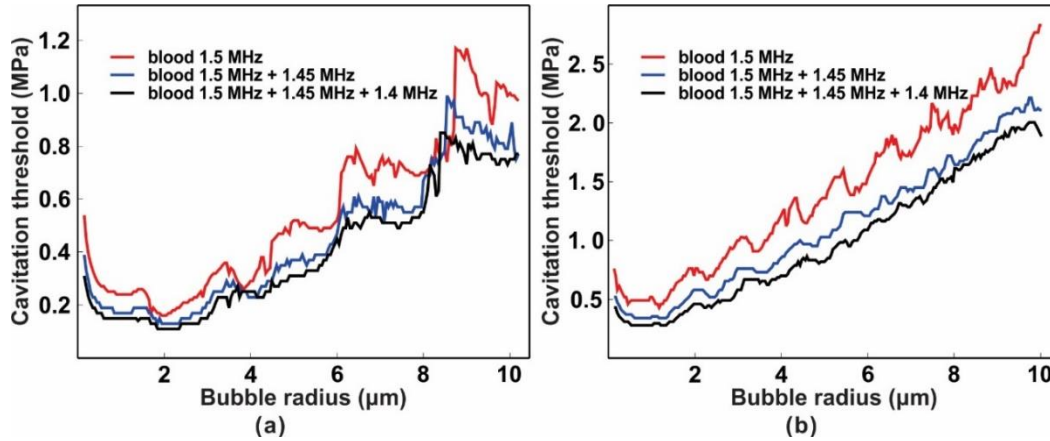


Fig 2. Inertial cavitation thresholds of single-, dual-, and triple-frequency excitations. (a) the criterion of $R_{max} = 2R_0$ and (b) the criterion of $\frac{dR}{dt} = -c$. Reprinted from [43].

Next, the effect of variance in power allocation of individual components in the multi-frequency signal was studied. One comparison of such permutations is shown in Figs. 3 (a) and (b).

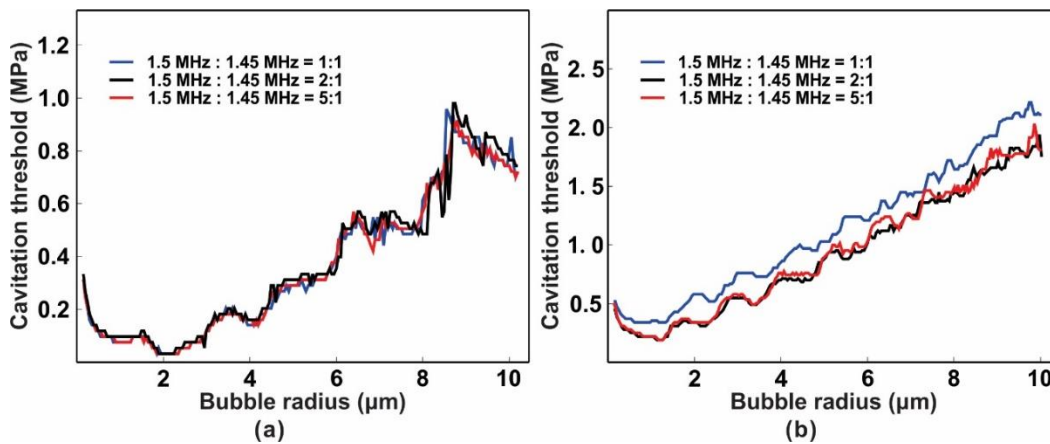


Fig. 3. Inertial cavitation thresholds of dual-frequency excitations with different power allocations, in blood using (a) the criterion of $R_{max} = 2R_0$ and (b) the criterion of $\frac{dR}{dt} = -c$. Reprinted from [43].

This lends to an understanding of the trade-offs that contributions of energy of each frequency component make in producing the cavitation effect. Evidently, no appreciable difference in cavitation threshold was seen using the $R_{max} = 2R_0$ criterion. However, while using the $\frac{dR}{dt} = c$ criterion, it was observed that the signal having equal power allocation among its components yields higher cavitation threshold. Overall, however, variation in power amplitudes of individual frequencies between ratios of 1:1, 2:1 and 5:1 for the dual-frequency signal is trivial doesn't yield a tangible advantage in lowering cavitation threshold.

1.2.2 Experimental considerations in HIFU-mediated thrombolysis

Several important factors bear influence in the thrombolytic effect of HIFU sonication. They are specific to the objectives and the parameterized-study at hand. A few of them are discussed here.

Meunier et al. [46] determine the efficacy of thrombolysis by light transmission through the clot and quantify intensity by Beer-Lambert's Law. Edge-detection was used to find the boundaries of the clot and find average clot thickness. It was found that the normalized average clot width, after 30 min of exposure to ultrasound and rt-PA, is much smaller at a duty cycle of 20% than at 10% duty cycle ultrasound, as shown in Figure 4.

Sutton et al. [19] used a contrast agent (Definity, Lantheus Medical Imaging; Billerica, MA) and rt-PA in vials made of two different materials and produced clots with differing compositional properties, as determined by routine scanning electron microscopy and histology. Clots were deployed in an ex vivo porcine thrombosis model and exposed to an intermittent ultrasound scheme previously developed to maximize stable cavitation while acoustic emissions were detected.

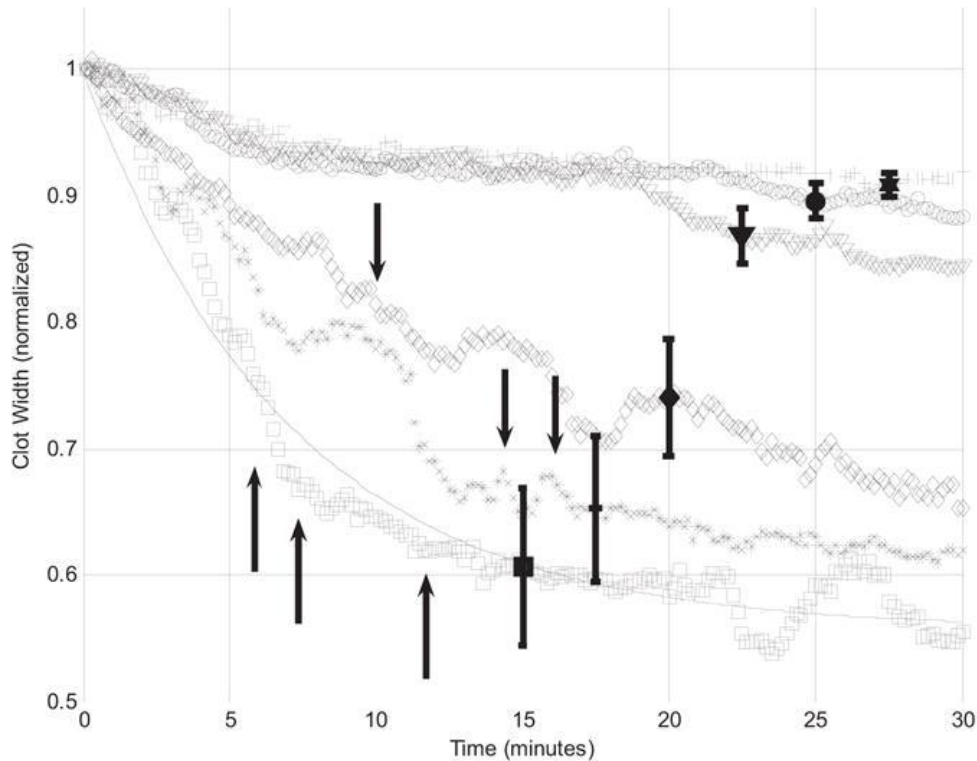


Figure 4. Normalized average clot width vs. time for clots exposed to ultrasound enhanced thrombolysis at different duty cycles. Normalized average clot width is shown for control (+), sham (inverted triangle) and treatment trials with duty cycles of 10 % (open circle), 20 % (open diamond), 50 % (asterisk) and 0% (open square). The solid line is a best-fit curve, to clots exposed to rt-PA and 80% duty cycle ultrasound. Black vertical arrows mark incidences of clot dissolution. (Meunier *et al.* 2007)

It was found that unretracted clots experienced greater enhancement of thrombolysis in the presence of rt-PA and ultrasound, when compared with treatment with rt-PA alone, as shown in Figure 5. In these clots, microscopy revealed loose erythrocyte aggregates, a significantly less extensive fibrin network and a higher porosity, which suggests an increased penetration of thrombolytic agents by cavitation. There are also variations in the types of lytic agents used in sonothrombolysis. Ultrasonographic molecular imaging in histological sections of thrombi in murine animals treated with Abciximab immunobubbles and ultrasound reveal greater disintegration when compared with thrombi in control groups. Specifically, 2 MHz ultrasound in

combination with abciximab immunobubbles was found to induce faster thrombolysis without lytic agents than insonation of non-specific immunobubbles.

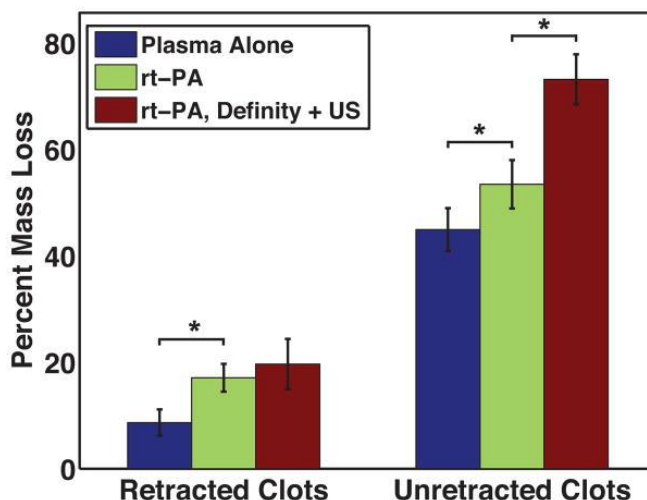


Figure 5. Thrombolytic efficacy, as determined by percent mass loss, for plasma alone, 3.15 $\mu\text{g}/\text{mL}$ rt-PA, and rt-PA, Definity + ultrasound treatments (Sutton *et al.* 2013).

Further, it is suspected that although an exact reason is unknown, the co-localization of a thrombus ‘pit’ with the oscillating microbubble suggests a causal relationship [47]. This action has been investigated with high-speed microscopy as shown in Figure 6.

Further, as shown in [63] the microscale interactions between individual MBs and fibrin clots depend on function of bubble size, exposure conditions and clot type which may be either coarse or fine. It was seen that, for fine clots, a substantial fraction of penetrating bubbles induced fibrin network damage. Further, the uptake of nanobeads was promoted. In coarse clots, however, MB penetration occurred at a faster rate and at lower pressures than in fine clots.

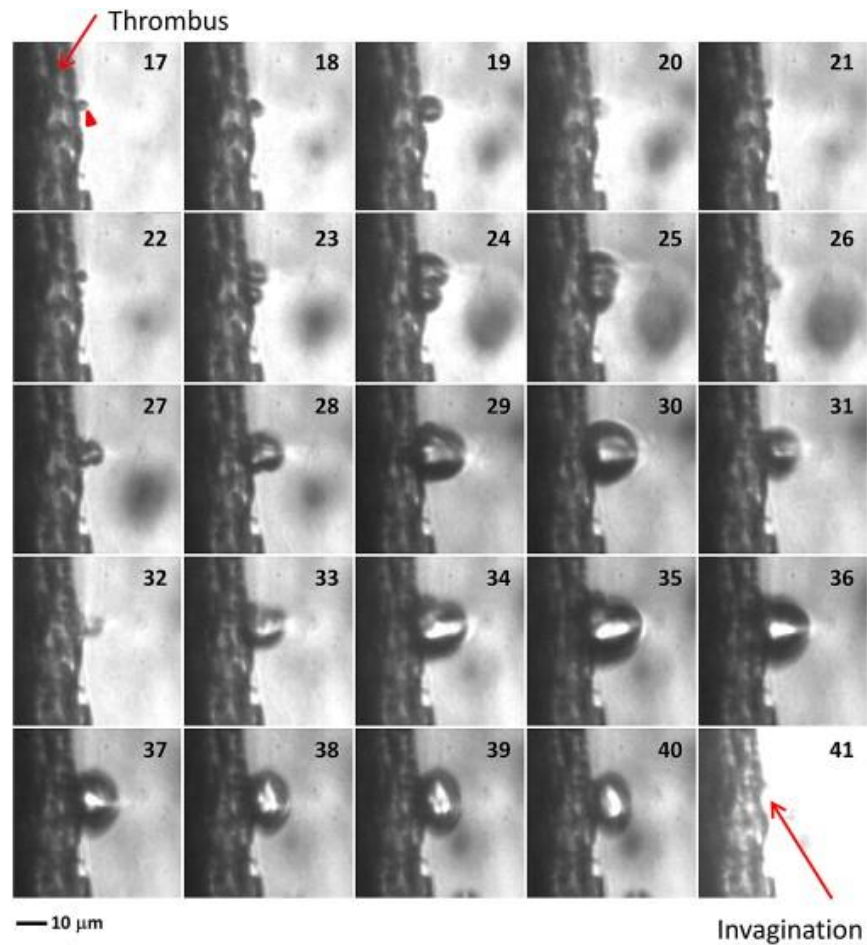


Figure 6. Sequential bright-field microscopic images of a microbubble adjacent to a thrombus during ultrasound delivery (1 MHz, 1.5 MPa) recorded at 5 Mfps. The thrombus appears on the left (*arrow*), and the microbubble in contact with the thrombus is on the immediate right (*arrowhead*). The time elapsed between successive frames is 200 ns. The microbubble expands and contracts, and after the microbubble has disappeared, there is a residual “pit” left at the thrombus site where the microbubble had been located (Chen *et al.* 2014 [48]).

Plausibly, repetitive agitation of a thrombus surface by vibrating microbubbles influences local fluid flow and, therefore, enhances transport of endogenous or exogenous lytic agents into the thrombus. The finding of the translational motion of microbubbles toward the thrombus also warrants further exploration of the role that Bjerknes forces may play in sonothrombolysis. This suggests that dual-frequency irradiation may produce more bubble nucleation as the result of the low-frequency stimulation and the intensified Bjerknes force [48], yielding enhanced thrombolysis.

CHAPTER 2

Design of the HIFU-induced thrombolysis experiment

2.1.1 Clot preparation

The procedure for preparing the blood clots is similar to that used in prior practice [22]. Bovine blood, anticoagulated with Anticoagulant Citrate Dextrose (ACD) solution (Citra Labs, Braintree, MA), is used. It is treated with a 2.75 % weight/volume calcium chloride (CaCl_2) solution (SC-10-1, Fisher Scientific, Fair Lawn, NJ) which serves as a coagulant. One part by volume (5 ml) of this CaCl_2 solution is added to 10 parts by volume (50 ml) of bovine blood. This mixture is sealed in clear tubing (Tygon S3™ – Fisher Scientific, Hampton, NH) which is 1/8” in inner diameter and 3/16” in outer diameter. The length of each tube facilitates study of clots with an effective length of 9.5 - 10 cm. A suture, passing coaxially through each tube, is used to anchor the clot in its holder and prevents it from being drained away by flowing water simulating fluid in a blood vessel.

The filled tubes are immersed in a 37 °C water bath for three hours and then stored at 4 °C for over seventy-two hours for complete clot generation and retraction. Each clot, embedded in its tube, is cylindrical in shape with a mean diameter of 3 mm. Further, before each trial, the clots are again immersed in a water bath for an hour and are then loaded into the clot holder before treatment with HIFU.

2.1.2 Microbubble solution preparation

Microbubbles are produced from lipid solutions as described in [43]. The radius of each MB is $0.9 \pm 0.45 \mu\text{m}$ at a concentration of 10^{10} MBs/ml, after activation. 1 ml of MBs is dissolved in 10 ml of saline solution to achieve a concentration 10^9 MBs/ml. To obtain other concentrations, different amounts of saline solution would be used. Before the trials, the MBs are activated using a shaker (Bristol-Myers Squibb Medical Imaging, Inc. N. Billerica, MA) for 45 seconds.

2.2 Experimental apparatus and data acquisition

Figure 7 shows the schematic for the experiment. Each clot is stationed within a water tank at an ambient temperature of 37 °C. The clot holder and custom fixtures are 3-D printed from Polylactic Acid thermoplastic. Multiple-axes position control of the clot relative to the HIFU transducer is achieved by a XYZ translation stage (VXM-3 series, Velmex Inc., Bloomfield, NY, USA) using three stepper motors (VEXTA stepper motors and model D6C-6.3F dampers, Oriental Motor Co., Tokyo Japan).

To record and timestamp the effect of different permutations of driving pressure and frequency, a video camera (Canon VIXIA HF R72 – 3.28-megapixel camcorder) is used. It is stationed directly above the clot and exterior to the tank housing the clot and transducers. Notably, it is mounted on the x-stage and slides along with the clot holder. It, therefore, always keeps the entire length of the clot in view. The camera has a frame rate of 30 frames/sec and accounts for a total of roughly 16,500 frames per trial, which are subjected to post-processing.

The HIFU transducer (Blatek, Inc., State College, PA) used for sonothrombolysis has an aperture diameter of 29.5 mm and a focal length of 30 mm. It has a center frequency of 1.5 MHz and a –6 dB beam width of 1.13 mm. Since the clot traverses along the x-axis, the transducer is kept stationary. The transducer forms an ultrasound beam which is perpendicular to the length of the clot with a constant horizontal angle of incidence. During the trials, the clot slides axially (along x-axis) and sites are sonicated at intervals of 8 mm.

During the experiment, an arbitrary waveform function generator (AFG 3101, Tektronix, Beaverton, OR, USA) produces pulses with a 1-ms period and at a duty cycle of 10 % . The pulses

generated are subsequently amplified by a RF power amplifier (240L, Electronics and Innovation, Rochester, NY, USA) which couples the function generator to the transducer.

A high-intensity hydrophone (HNA-0400, ONDA, Sunnyvale, CA) is used to calibrate the PNP amplitudes at the focus of the HIFU transducer. The cavitation signal single-frequency sonication and dual-frequency sonication is received by a 10 MHz focused transducer T2 (Olympus IMS, Waltham, MA) and a pre-amplifier (AH-2020, ONDA, Sunnyvale, CA) couples it to a data acquisition card (GaGe Oscar CompuScope 14-bit digitizer, Lockport, IL). During detection of cavitation signals, data is sampled every 10 s, and a total of 10 samples are taken. During data acquisition, 4 bursts at a sampling rate of 50 MHz and 4 ms in duration are used. In each case, signals recorded in the time-domain are transformed into frequency-domain for better observation.

2.3 Flow system

In contrast with previous studies [40], the objective of this study is to simulate the effect of microbubble-mediated HIFU-induced thrombolysis under the influence of dynamic fluid akin to that in a blood vessel. A simple flow system is designed to facilitate this. A peristaltic pump (13-876-1-Variable Flow Peristaltic Pump, Fisher Scientific, Hampton, NH), with a volume flow rate of 0.4 ml/s, imparts an average speed of 23 cm/s to 94 cm/s to the flowing water at the site of the clot. This is, however, contingent on the mean diameter of each clot. The MBs are drawn into a 30-ml syringe (Henke Sass Wolf, Tuttlingen, Germany) which is installed on a micropump (DUAL-NE-1010-US, New Era Pump System Inc., Farmingdale, NY). The micropump injects the microbubble solution in an intravenous fashion to the site of the clot. The micropump is configured to have a flow rate of 100 μ l/min during the entire process [49]. During the experiment, the peristaltic pump supplies water from a tank and through the tubing to the clot which is held stationary by its embedded suture while the micropump supplies MBs.

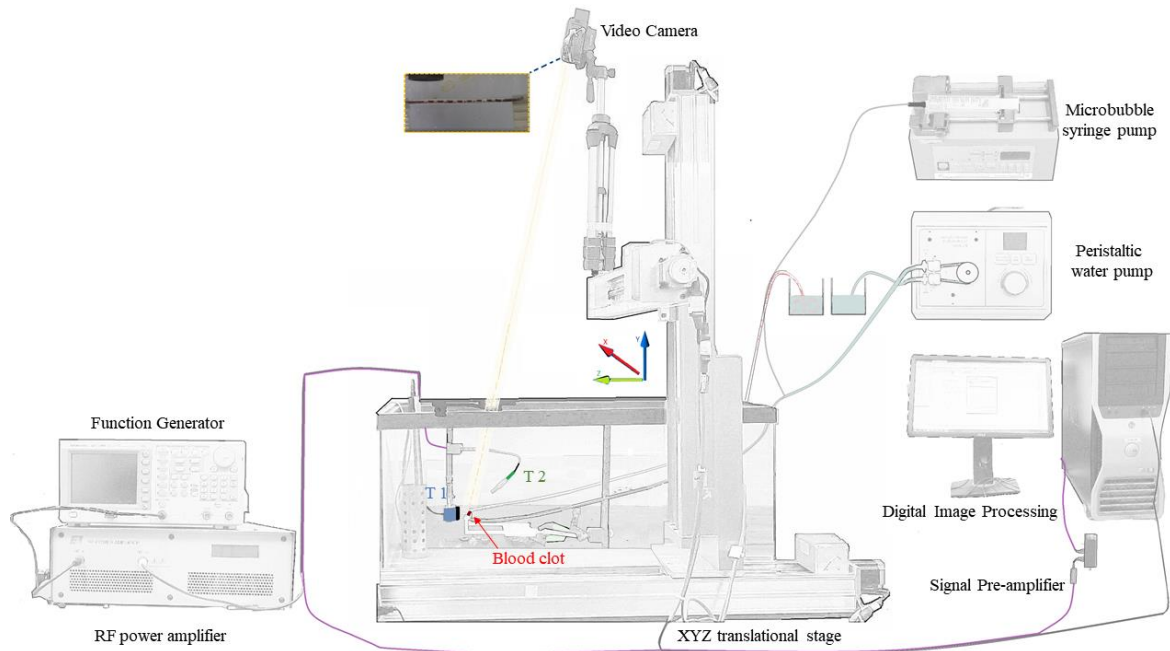


Fig. 7. *In vitro* experimental setup to examine microbubble-mediated HIFU-induced thrombolysis.

2.4 Alternate motorized arrangement for mounting and focusing the HIFU transducer

The original arrangement was substituted with another configuration employed in some trials to facilitate more accurate focusing of the HIFU transducer (T2). This setup involves the use of a motorized robotic arm as shown in Figure 8. It consists of 6 servo-motors which impart 5 degrees of freedom.

The six commercial servos and brackets were obtained from the Tinkerbot assembly accessories marketed by the Arduino open source computer hardware and software company. The servos were programmed and interfaced using MATLAB[®]'s Arduino Toolbox's subroutines. An Arduino Uno microcontroller is used to relay the angular inputs, parsed as strings, from the MATLAB[®] workspace to Arduino's Integrated Development Environment (IDE). One example of code developed for this purpose is included in Appendix A (c). A separate modular circuit board is mounted on the main Uno board and provides the COM-port connection (USB serial port) and

requisite power connection to the 6 motors which cannot be independently provided by the micro-controller operating on a 5-V supply. The base, upper-arm, elbow, fore-arm, wrist and end-effector are enclosed in a nitrile-coated sheath (26-inch Showa Atlas® 772 long sleeve glove) to allow for underwater operation. Transducer T2 is integral to the end effector and is mounted using a custom 3-D printed housing made of NinjaFlex® TPU 3-D printing filament (NinjaTek, Manheim, PA). The sphere of influence of the arm is determined by the range of angular inputs to each link of the articulated arm. The relative positions of the simplified arm, clot-holder and fluid inflow and outflow tubing is shown in this new configuration is Fig. 8.

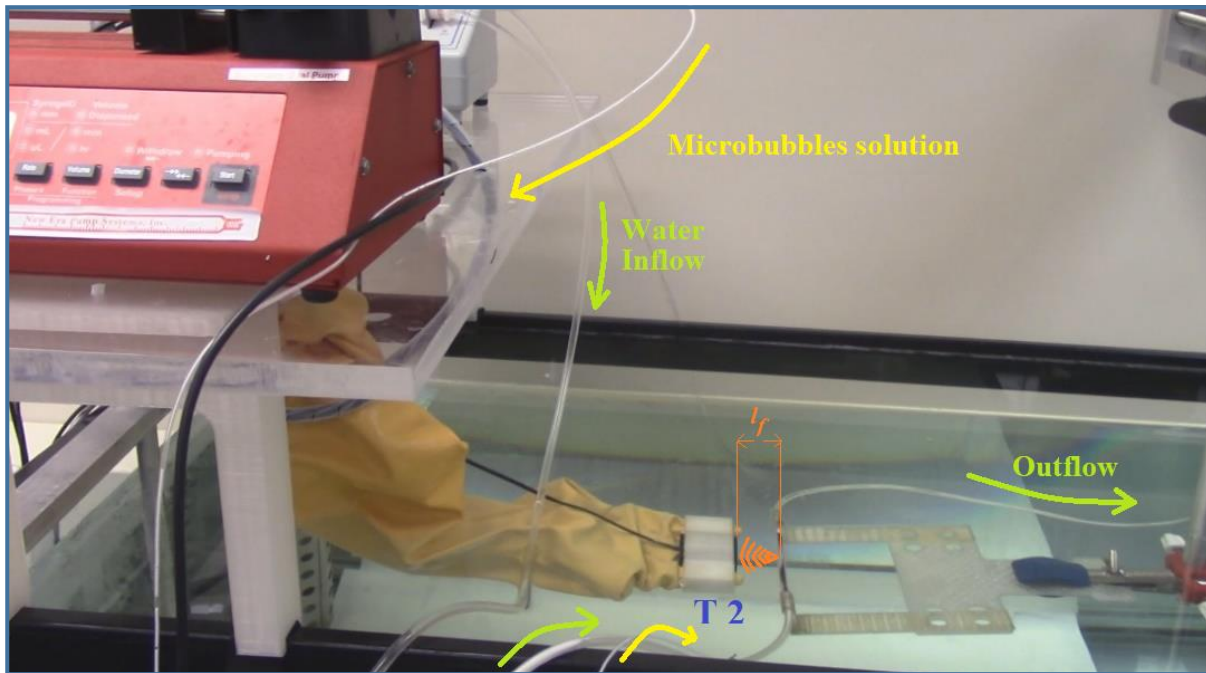


Fig. 8. A second arrangement consisting of a motorized arm, HIFU transducer, clot holder and flow system in the MB-mediated thrombolysis experiment.

The composite arm is shown in Fig. 9 (a) and an example of its 2-D workspace (YZ plane) is shown in Fig 9 (b). The zone of highest resolution is highlighted in orange and represents the preferable location of the clot-holder during the thrombolysis experiment. Simplistically, the coordinates of the end-effector (outermost plane of the transducer) in the X-Y-Z co-ordinates is modelled by forward kinematics given as follows.

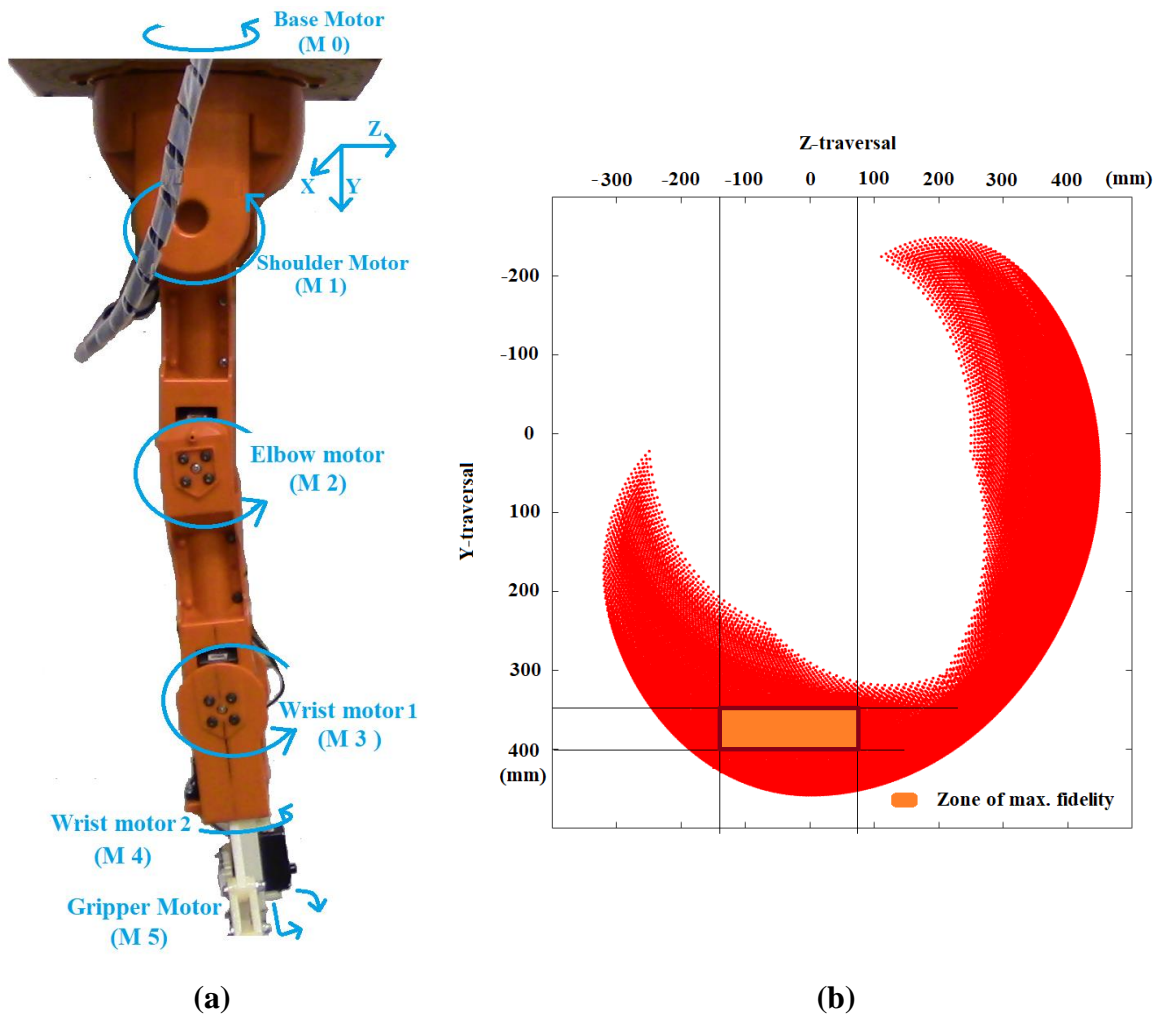


Fig. 9. Articulated, Arduino-controlled arm employed for better focusing (a) Relative position of motors M2 and M3 used in the shortened configuration. (b) 2-D workspace of the end-effector (transducer T2) in the YZ-plane.

It is assumed that the origin of the co-ordinate axes corresponds to the location of the shoulder-motor (M1). The focus-length of the 1.5 MHz-centred transducer is l_f . Denoting arm segments

corresponding to the upper-arm, elbow and wrist as l_{up} , l_{elb} and l_{wr} the input angles effected by the shoulder, elbow and wrist motors, M1, M2 and M3 as θ_{sh} , θ_{elb} and θ_{wr} , it can be shown that to maintain the wrist segment at an orientation parallel to the Z-axis and considering motion in only the Y-Z plane, θ_{sh} , θ_{elb} and θ_{wr} would assume a relationship given by

$$\theta_{sh} + \theta_{elb} + \theta_s = 90^\circ \quad (1)$$

The co-ordinates of the tip of the end-effector (transducer-housing) would then be

$$Y = \cos \theta_b [l_{up} \cos \theta_{sh} + l_{elb} \cos(\theta_{sh} + \theta_{elb})] \quad (2)$$

$$Z = l_{up} \sin \theta_{sh} + l_{elb} \sin(\theta_{sh} + \theta_{elb}) + l_{wr} \quad (3)$$

$$X = -\sin \theta_b [l_{up} \cos \theta_{sh} + l_{elb} \cos(\theta_{sh} + \theta_{elb})] \quad (4)$$

Practically, since the XYZ-stage allows traversal in the x-axis, the arm may only be used for greater mobility in the YZ-plane. This greatly simplifies calculation of arm's dynamics and the resultant arm may consist of as many as only two motors and brackets which support this configuration. In the underwater trials, rotation of the base is, therefore, unnecessary and the upper arm may also be kept stationary to reduce underwater vibration induced by servo-action. The numeric values of the various arm-segments and range of input angles is given in Table 1.

Table 1. (a) Length of motorized-arm segments, and (b) Range of angular operation for base, shoulder, elbow and wrist motors.

Arm-segment	Length (mm)	Motor	Range of rotation
l_{up}	130.4	θ_b (M0)	-15° to 15°
l_{elb}	128.1	θ_{sh} (M1)	0° to 75°
l_{wr}	169.2	θ_{elb} (M2)	0° to 75°
l_f	30	θ_{wr} (M3)	-75° to 75°

(a)

(b)

CHAPTER 3

Experimental quantification of clot dispersal rate and indentation efficacy

Distinct cases for permutations of HIFU PNP/power and driving frequency (SFFU at 1.5 MHz and DFFU at 1.45+1.5 MHz) are evaluated. The desired PNP is produced by the corresponding input voltage. Note that, similar to previous studies [22], the PNP values listed throughout the paper are for SFFU only, while DFFU must yield a different PNP in order to have the same power as the SFFU. Having equal output acoustic power is essential for comparisons between the two types of excitations. The thrombolysis efficiency results are always compared under the same power between DFFU and SFFU.

During each trial of the experiment, the action of the HIFU transducer is transferred to points 8 mm in separation along the length of the blood clot. Each point of action is given approximately 60 seconds before the clot is moved to the next position. To reflect the efficiency of some particular PNP-frequency combinations, in the event that the clot at that point of action is completely dispersed, the clot is moved ‘prematurely’ to the next position without depleting the maximum allotted time of 60 seconds. An average of 10 points of action are subjected to treatment for each clot. Further, the MBs are continuously injected into the water stream at one end of the tube which houses the clot. A visualization of the method used to quantify a clot’s degradation rate is shown in Fig. 10. During post-processing, each image depictive of the clot’s condition at a particular timestep is analysed using MATLAB[®]’s (Mathworks, Natick, MA) Digital Image Processing Toolbox (ver. 2017a). The code used for its implementation is given in Appendix A (a) and (b).

The first parameter considered is the total blood clot content at each time step. As Figs. 10 (a) and (b) show, to facilitate this, each colour image is converted to a binary (black/white) image to isolate

the clot silhouetted against the lighter background of the water-tank’s floor. This is based on red-green-blue threshold criteria to clearly characterize the clot. The image is cleaned by removing small blobs and smoothing coarse borders based on pre-set size and roughness thresholds. The pixels embodied by the clot progressively dwindle in number (Fig. 7 b) and at each instance, this is compared to their number in the original, untreated clot (Fig. 7 a).

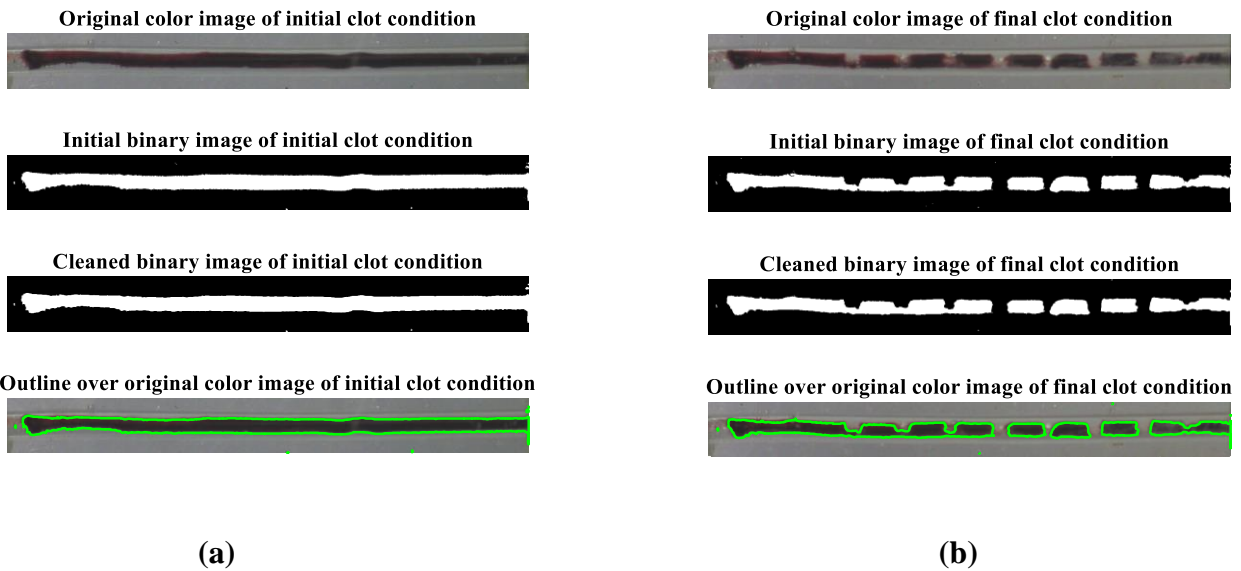


Fig. 10. Image processing of (a) an untreated clot and (b) a clot subjected to MB-mediated HIFU (1.45 MHz + 1.5 MHz).

This yields the percentage of remaining clot in the tube. A median filter is then used on the collective data at the end of the trial to remove the small variance in results due to noise. This establishes a quantitative assessment of the trend in the clot’s mass loss. This, compared to the approach where only the image of the final moment of the clot is used to extract the mass loss rate [9, 39], provides a more accurate time-transient estimation of the mass loss rate.

A second parameter is used to gauge the efficacy of HIFU treatment at each site of treatment. The percentage of clot dispersed at each point of action is estimated by a process of delineating the boundaries of individual segments of the resultant segmented clot, i.e. both the exterior boundaries

of the segments, as well as boundaries of holes inside these segments, in each binary image are traced and arrays of boundary pixel locations are derived. Their overlays on the original colour image are shown in Fig. 10 (b). To study the effect of MB-mediated HIFU treatment at each point of action, the left and right limits of the effected indentation are queried, and the removed portion of the clot is compared with the original clot within those limits. An illustration of this method for the sub-segment corresponding to the second point of action of a clot is shown in Fig. 11. Representative images for all configurations of permutations of PNPs and SFFU and DFFU sonication are included in Appendix B.

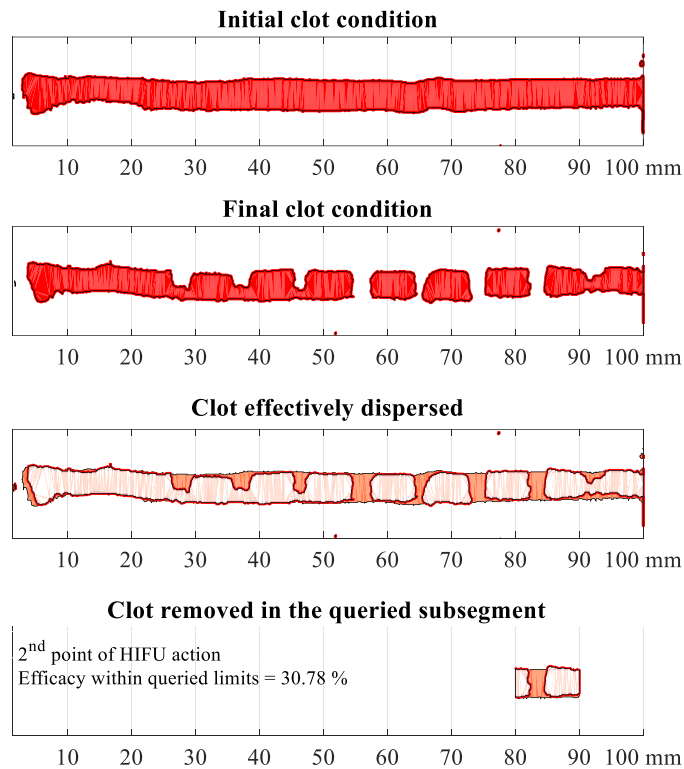


Fig. 11. Image processing and estimation of efficacy of microbubble-mediated HIFU treatment for individual indentations along the length of the clot for a representative case of DFFU treatment.

CHAPTER 4

Results and discussion

4.1 Experimental results of MB-mediated thrombolysis using the flow model

The efficiency of thrombolysis is assessed by two parameters: percentage clot content and indentation size, for five cases of PNPs for both SFFU and DFFU under MB mediation. The results of image post-processing now follow.

Fig. 11 was shown to illustrate the method by which the size of indentation caused by variations in PNP amplitude under SFFU and DFFU treatment can be estimated. Fig. 12 shows the dynamic disintegration of blood clots due to ultrasound under varying PNPs at a MB concentration of 10^9 MBs/ml. Within the time-window of each trial, as shown in Fig. 12, it is noted that the percentage of remaining clot, when subjected to SFFU, has little effect for PNP lower than 3.5 MPa while the percentage of remaining clot, when subjected to DFFU begins to show greater effect at 3.0 MPa. The relatively small portion of disintegrated clot (15%-25% in many cases at around 550 sec), is indicative of site-specific treatment along the length of the clot. The areas of clot not subjected to HIFU and in between the treatment sites remain largely unaffected (no sonication). We could have removed the clot more thoroughly by reducing the scanning step size. This, however, would make the image processing more challenging. Overall, no significant change on the slope of the clot percentage curve is observed, especially in Fig. 12 (c)-(e) where thrombolysis is clearly observable. However, inflections can be seen at instances of time when a new site is subjected to HIFU. At the highest power corresponding to an SFFU PNP of 4.5 MPa, SFFU and DFFU perform similarly.

As Figs. 12 (b) and (c) show, MB-mediated DFFU sonication has a greater effect than SFFU at 3.0 MPa and 3.5 MPa and serve to benchmark the possible acoustic energy at which inertial cavitation is enhanced. The sudden drop of the DFFU curve at around 500 second in Fig. 12 (c) occurs because the clot was flushed away. For SFFU in the first two figures, the curves hover about 97-98 % due to inefficient thrombolysis. In this case, the median filter cannot easily calculate a value at a time-frame which is greater than that at a previous time frame and noise can affect the prediction. This is why the curves manifest slight fluctuations in Figs. 12 (a) and (b) and sometimes the curve even rises, which is non-physical. To further analyse the results, a comparative assessment is made for this MB concentration, as shown in Fig. 13 (b). Here, the control group refers to a reference case wherein HIFU action is absent and the clot is subjected to a free stream of water and injected microbubbles. This serves to establish the efficacy of each permutation of ultrasound PNP and frequency component(s).

The second parameter used for analysis, i.e. the size of indent (averaged over all targeted areas), also shows interesting trends in Fig. 13 (a). For instance, the indentation caused by DFFU excitation increases abruptly from a PNP of 2.5 MPa to 3.0 MPa. SFFU, however, effects a similar increase in indent size in a PNP range of 3.0 MPa to 3.5 MPa. Note that the portion of clot dissipated here in Fig. 13 (a) represent the portion of a single dent to the size of the whole clot, which results in its small quantity (<5%).

The rate of dissipation calculated from a linear fit for each case shown in Fig. 12 is illustrated in Fig. 13 (b). As can be seen, in general, DFFU engenders a faster rate of clot dissipation in comparison with SFFU, on increasing the power. This is most pronounced for the case of 3.0 MPa. In an attempt to substantiate these observations, the cavitation signals for SFFU and DFFU for varying PNPs are then measured in Fig. 14, using signal acquisition and processing techniques

similar to that in [40]. Spectral analysis shows that the magnitude of broadband noise for dual frequency excitation rises strongly for a PNP of 3.0 MPa and that the magnitude of broadband noise for single frequency excitation rises strongly for a PNP of 3.5 MPa.

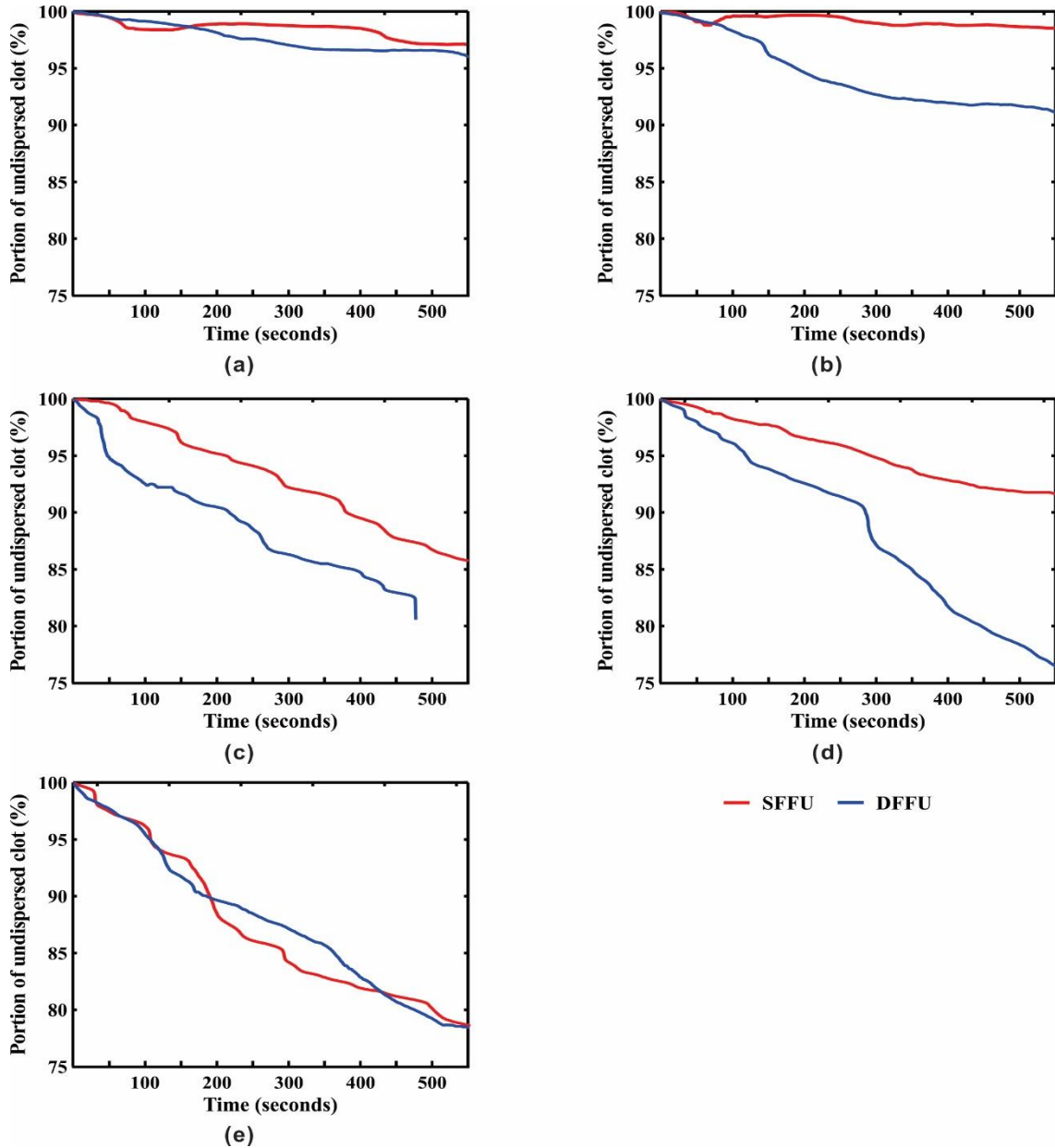


Fig. 12. Time-transient dissipation of blood clot when subjected to microbubble-mediated (at 10^9 MBs/ml) SFFU at 1.5 MHz and DFFU of 1.45 MHz + 1.5 MHz, for PNPs of (a) 2.5 MPa, (b) 3.0 MPa, (c) 3.5 MPa, (d) 4.0 MPa, and (e) 4.5 MPa.

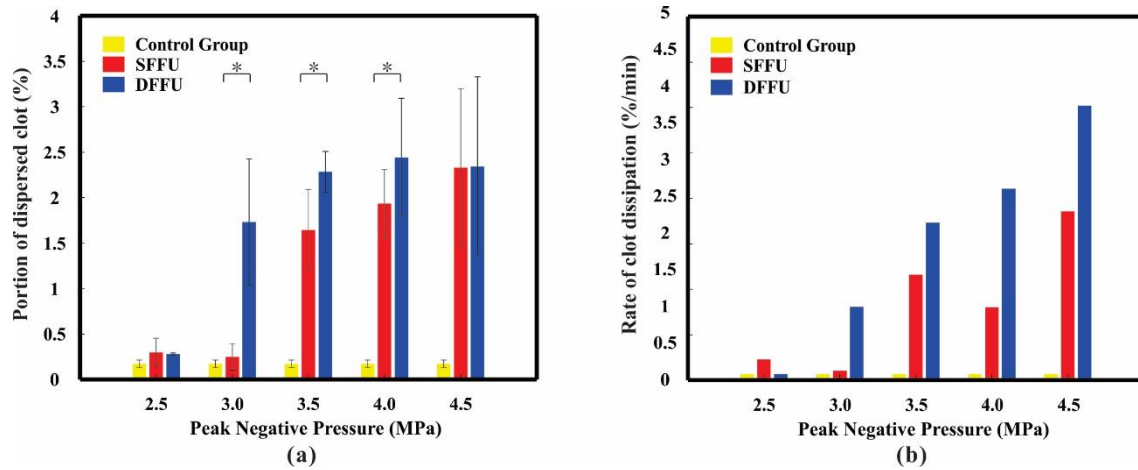


Fig. 13. Comparison of (a) indentation size as a percentage of initial clot, for varying PNPs for MB-mediated (10^9 MBs/ml) SFFU (1.5 MHz) and DFFU (1.5 MHz + 1.45 MHz) and (b) overall rate of dissipation during each permutation of the experiment. (* p-value < 0.05)

This again demonstrates that dual-frequency excitation effects a lower cavitation threshold and this is correlated with the enhanced thrombolysis. It is noted that in Fig 13 (b), the SFFU efficiency at 4.0 MPa is less than 3.5 MPa. This is because during the dissipation rate analysis, we had a few large dents for the 4.0 MPa SFFU treatment but the linear fitting cannot capture this accurately, resulting in a slope smaller than expected.

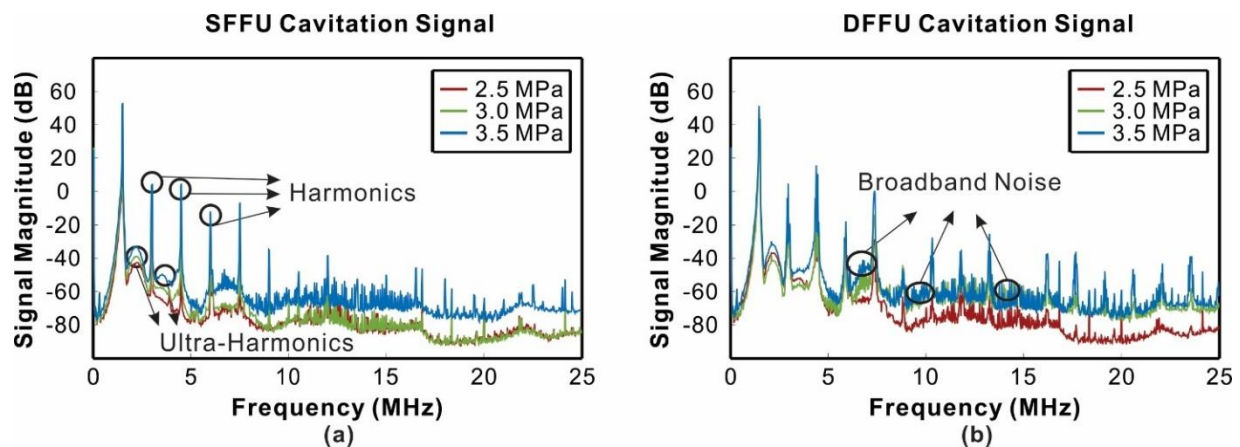


Fig. 14. Cavitation signals for (a) SFFU and (b) DFFU for various PNP amplitudes at a microbubble concentration of 10^9 MBs/ml.

Clot dissipation at a PNP of 3.5 MPa is further examined. The experiment is repeated at this HIFU energy, though with varying microbubble concentration. Here, the effect of concentrations of

0 MBs/ml, 10^8 MBs/ml, and 10^9 MBs/ml are compared. From Fig. 15, it may be discerned that at a concentration of 0 MBs/ml, i.e. HIFU treatment without MB mediation, DFFU has a slight thrombolytic effect while SFFU shows no appreciable effect on the clot. This indicates SFFU does not reach the cavitation threshold that stimulates thrombolysis. Further, when the MB concentration is increased to 10^8 MBs/ml, both SFFU and DFFU excitation dissipate the clot more efficiently than without MBs. This would suggest that MBs generate more cavitation nuclei and, hence, stronger inertial cavitation activity. An attempt to further increase the concentration would be instructive. The thrombolysis efficiency at a concentration of 10^9 MBs/ml in Fig. 12 (c) is about the same as 10^8 MBs/ml concentration. As Fig. 16 shows, it is observed that the rate of clot dissipation is slightly worse than that of 10^8 MBs/ml. This is in opposition to our general hypothesis that more MBs would produce a higher thrombolysis efficiency. As [40] and [41] suggest, it is plausible that the aggregation of MBs at such a concentration could cause an acoustic shadowing effect, whereby most of the incident power would be reflected rather than penetrate through these bubbles. Effectively, this inhibits the transmission of acoustic energy to the site of the clot and adversely affects the thrombolysis efficiency.

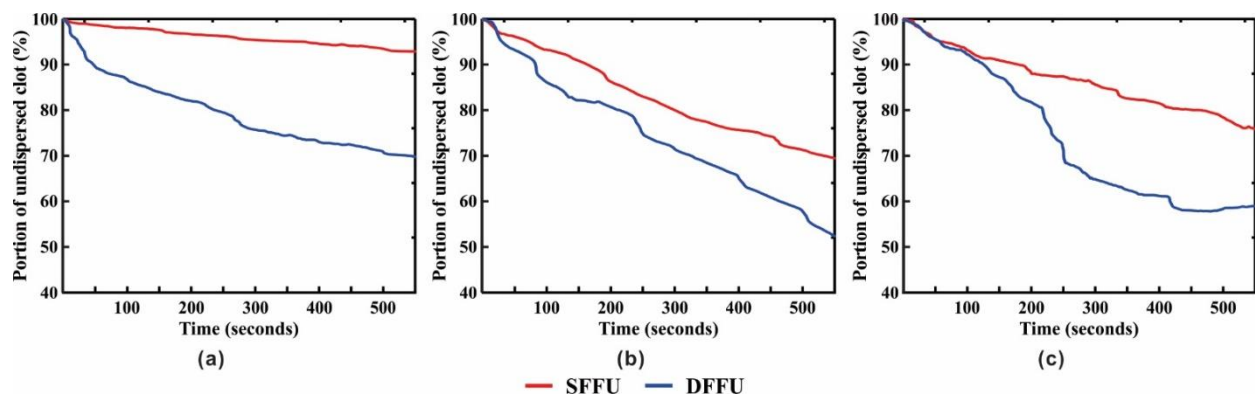


Fig. 15. Time-transient dissipation of blood clot subjected to microbubble-mediated SFFU (1.5 MHz) and DFFU (1.45 MHz + 1.5 MHz) at a PNP amplitude of 3.5 MPa for microbubble concentrations of (a) 0 MBs/ml, (b) 10^8 MBs/ml and (c) 10^9 MBs/ml

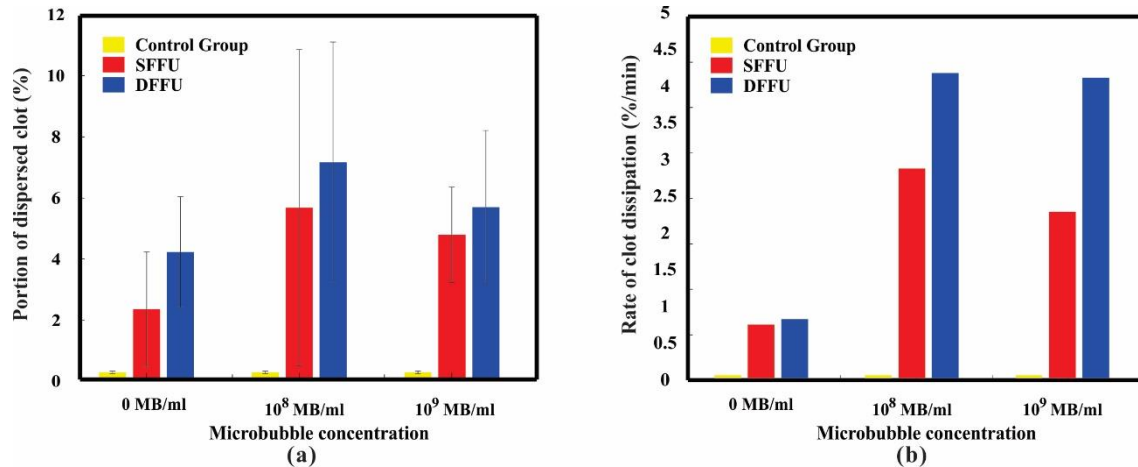


Fig. 16. Comparison of (a) indentation size as a percentage of initial clot, with variance in microbubble concentrations for SFFU (1.5 MHz) and DFFU (1.5 MHz +1.45 MHz) excitation and (b) overall rate of dissipation for each permutation of the experiment at a PNP amplitude of 3.5 MPa.

It may be noted that in these separate iterations of the experiment, i.e. trials with varying PNP and constant concentration and trials with variation in MB concentration, batches of clots have mutually distinct physical conditions, albeit homogenous condition within each batch. This is important as experimental evidence shows that clot retraction [19] can decisively affect thrombolysis efficiency and comparison of thrombolysis efficiency should be made only among cases of similar clot condition. This explains why Figs. 15 and 16 seem to indicate more efficient thrombolysis than Figs. 12 and 13 do, even for the cases where the ultrasound and MB parameters are the same.

4.2 An extended analysis for Nanodroplet-mediated thrombolysis using the flow model

A peripheral analysis was further performed after the efficacy of microbubbles was established. Here, the efficiency of phase-shift Nanodroplets (NDs) was evaluated. According to previous investigations [53-59], these nanometer-sized liquid droplets evaporate into micrometer-sized gas bubbles when exposed to HIFU. This is the outcome of the volumetric expansion due to the phase shift of liquid NDs. Typically, the time needed for this acoustic droplet vaporization (ADV) is a

few microseconds. In addition, some researchers [53,55] have investigated the relationship between ADV and inertial cavitation (IC) thresholds and they found that the ADV threshold occurred at a lower rarefactional pressure than the IC threshold, indicating that the phase transition occurs before cavitation events [53].

Plausibility of enhanced cavitation under treatment of 1: 100 volume ratio of ND solution to saline solution was investigated. Using the same procedure outlined in the treatment of clots subjected to MB-mediated thrombolysis, test conditions in this campaign included treatment at PNPs of 2.5, 3, 3.5, 4 and 4.5 MPa under (a) ND-mediated SFFU sonication, (b) ND-mediated DFFU sonication, (c) SFFU sonication without ND-mediation and (d) DFFU sonication without ND-mediation, at the flow rate of 100 μ l/min used in the MB-mediated experiment.

As Figs. 17 and 18 show, at this ratio, nanodroplets have an inconsistent effect for varying PNPs. Notably, similar to the MB-mediated trials, the undispersed clot in this analysis, at 3.5 MPa, is about 50%-70 %, in spite of greater precaution in ensuring a better transducer focus. The clot condition, therefore, seems to play a lesser role in this experimental set. It may be presumed that either the ND solution is highly concentrated and engenders the shadowing effect previously encountered for MBs or that the ND solution's concentration is too weak to cause definitive effect. However, unlike the experiment with MB-mediated thrombolysis, wherein visible accumulation of the MB solution at the walls of the tube at high PNPs, in the ND-mediated treatment, no such accumulation was visibly apparent even at high PNP. Therefore, the concentration of NDs at this 1:1000 volume ratio may be assumed to be less than optimal for enhanced thrombolytic effect. A further comparative study at higher volume ratios, say, at 1:10 and 1:5 ratio of ND-solution to saline solution may be necessary to conclusively estimate optimal conditions of PNP and multi-frequency combination for faster clot dissipation.

This corroborates uncertain trends in inertial cavitation detection (ICD) as observed in [53-55]. These indicate that while intensity of cavitation for the phase-shift NDs increased with time, the cavitation for lipid-shelled MBs grew to a maximum at the outset of the FUS exposure followed by a decrease when they were static in the vessel. However, the rate of increase in cavitation for phase-shift NDs and decrease of cavitation for the lipid-shelled MBs slowed down under the influence of fluid flow. For instance, in [55], it was noted that in a cylindrical cavity in an agar phantom, the normalized ICD value for the phase-shift NDs was 0.182 at a flow velocity of 5 cm/s and increased to 0.188 at a flow velocity of 15 cm/s. As the flow velocity increased to 20 cm/s, the normalized ICD was 0.185 and decreased to 0.178 at a flow velocity of 30 cm/s.

Interestingly, these observations would imply that the effect of the flowing phase-shift NDs, which vaporize into larger gas bubbles and act as cavitation nuclei, may be in opposition to that observed for lipid-shelled flowing MBs under HIFU exposure. It may also be noted that the preparation of nanodroplets requires precise process control. Therefore, any analysis of its efficacy may have contingency on minute inconsistencies of properties arising due to varying septum of the storage vials used for gas exchange in the preparation of the nanodroplets.

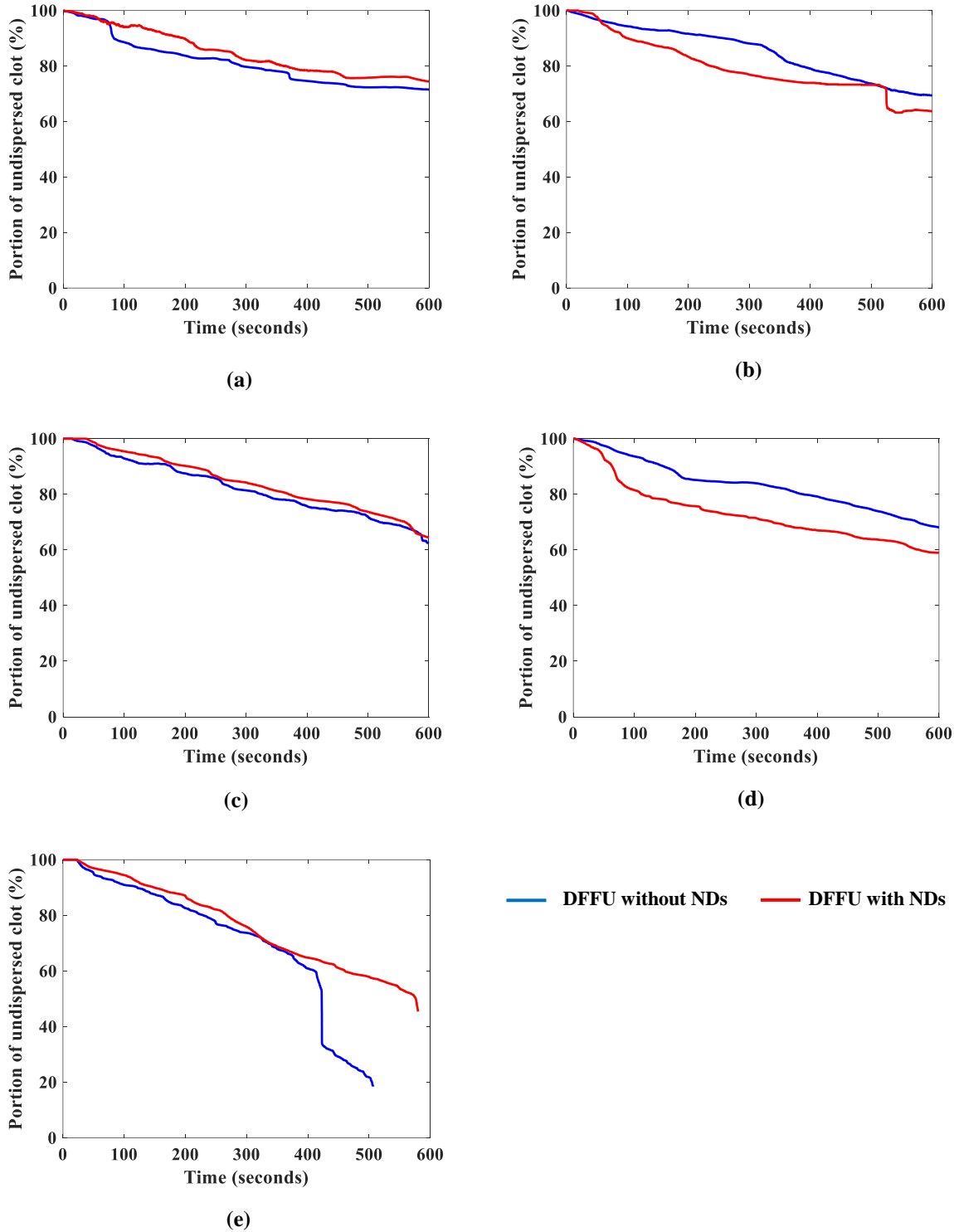


Fig. 17. Time-transient dissipation of blood clot subjected to DFFU (1.5 MHz + 1.45 MHz), with and without NDs for PNPs of (a) 2.5 MPa, (b) 3.0 MPa, (c) 3.5 MPa, (d) 4.0 MPa and (e) 4.5 MPa.

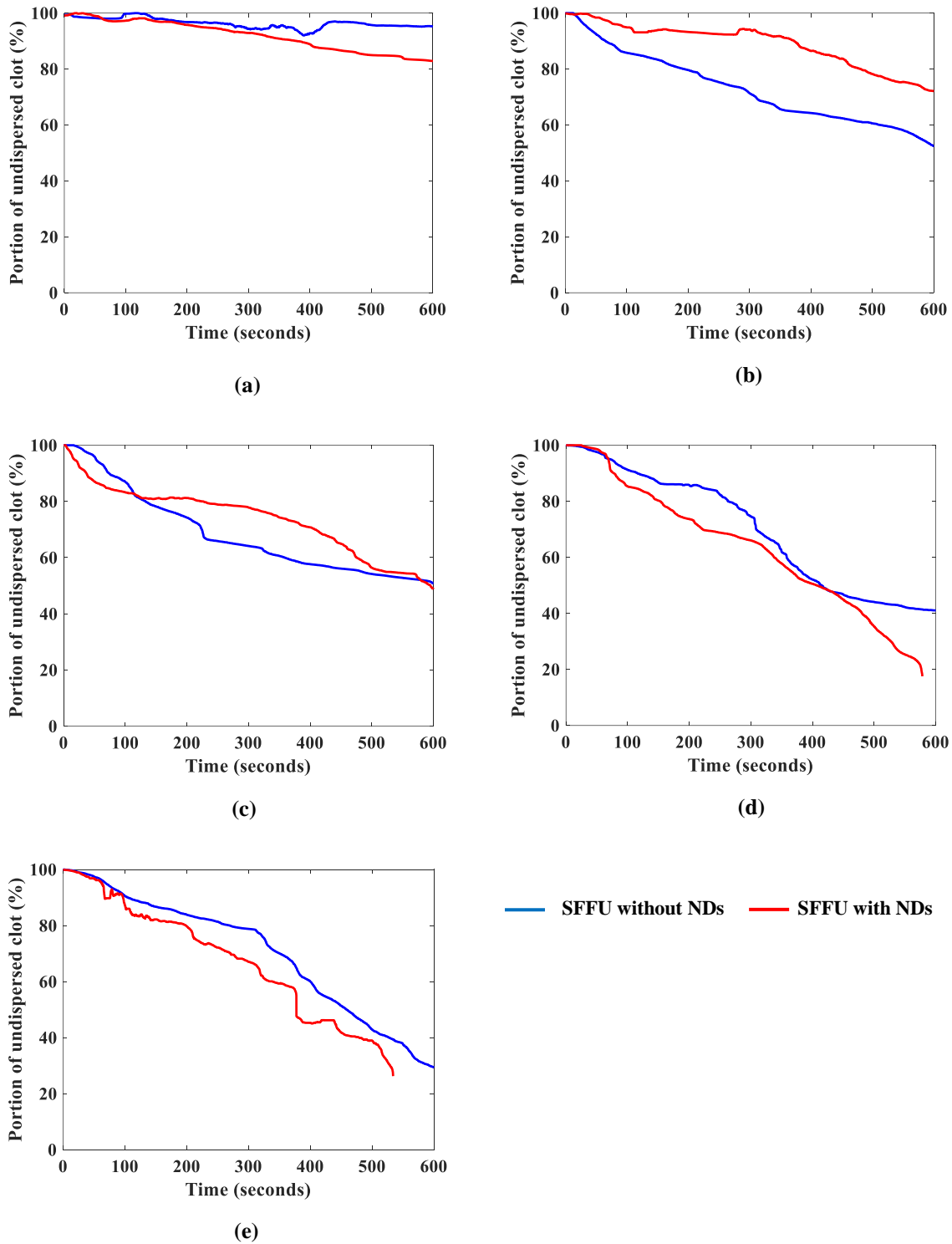


Fig. 18. Time-transient dissipation of blood clot subjected to SFFU (1.5 MHz), with and without NDs for PNPs of (a) 2.5 MPa, (b) 3.0 MPa, (c) 3.5 MPa, (d) 4.0 MPa and (e) 4.5 MPa.

This investigation indicates that the ADV threshold could be decreased if the duration of HIFU exposure is increased. Further, the effective duration of sonication needed for ADV of the phase-shift NDs is relative to the time during which the phase-shift NDs are exposed to the focal zone of the HIFU beam. This is determined by the flow velocity of the phase-shift NDs in their medium (saline solution). It is plausible that the duration of exposure in this experiment was shorter than the optimal time required to induce ADV for the flow velocity used in the experiment. However, at a higher acoustic power level, the ADV threshold was possibly lowered and consequently, the duration of FUS exposure needed for ADV of the phase-shift NDs was less than the corresponding PNP, thereby inducing ADV and inertial cavitation even at a higher flow velocity of the phase-shift NDs solution. Curiously, however, although HIFU treatment with phase-shift ND-mediation has greater effect than without ND-mediation, in most cases, SFFU has an observably better effect than DFFU. This would require a more in-depth insight into the mechanisms of interaction of NDs at the surface of the thrombus, rates of onset of ADV and, consequently, inertial cavitation thresholds to account for these paradoxical results.

CHAPTER 5

Conclusions and scope of future work

In this investigation, a customized *in vitro* setup was designed to evaluate the dynamic dissipation of thrombi under the action of water flow, DFFU, and microbubbles. The rate of clot disintegration was found to be contingent on the magnitude of acoustic energy and driving frequency (SFFU vs. DFFU). Our observations indicate that accelerated thrombolysis may be realized by the cavitation threshold of microbubbles excited by DFFU being lower than that of SFFU excitation. Digital image processing used to quantify the rate of clot dissipation and indentation size gives a real-time visualization of thrombolytic effect and time-transient variance in lytic sites exposed to HIFU. Additionally, this method is inexpensive and can be easily implemented to estimate the rate of clot disintegration and site-specific efficacy of HIFU treatment. This method may be further extended to incorporate real-time feedback and guide the transducer /phased array to achieve better focusing.

To comprehensively infer trends which lend to optimal HIFU input waveform parameters, trials were conducted using both DFFU and SFFU excitations, in concurrence with a range of input amplitudes. It is shown that dual-frequency excitation at energy levels identical to those of SFFU with PNPs of 3 or 3.5 MPa could feasibly promote thrombolysis for the specific clot and acoustic environment in this study. Further, at 3.5 MPa, it was sought to understand the effect of variation in MB concentration. Expectedly, it was found that the action of microbubble solution at a concentration of 10^8 MBs/ml is convincingly better than with no microbubbles. Interestingly, a ten-fold increase in MB concentration (at 10^9 MBs/ml) yields no tangible advantage, and this may be attributed to an acoustic shadowing effect despite the agglomeration of cavitation nuclei.

The analysis, using this flow model, was extended to the application of nanodroplets in HIFU-induced thrombolysis. The results of clot disintegration show peculiarities in the action of NDs due to plausibly discrete onsets their ADVs and inertial cavitation, which are dependent on PNPs and more importantly, flow speed which limits time of exposure to focused ultrasound in the vicinity of the thrombus.

Future work would include examining methods to further optimize HIFU for thrombolysis such as combining pulsed-laser and HIFU in a similar *in vitro* flow model to study acoustic-optical effects induced by high-power RF impingement. It is also anticipated that histological study would be performed to further examine the action of NDs within the clots and optimize the microtripsy effect of these thrombolytic agents. Further, variation in flow speed due to recanalization will be quantified using doppler velocimetry and real-time feedback will be used to implement deep learning algorithms to control the HIFU transducer or phased-array. The effect of downstream sediment would also be analyzed using particle sizing techniques. Future investigations would also include experimental trials in *in vivo* models using small animals such as rabbits, to demonstrate the true potential of DFFU-based thrombolysis and assess its safety.

REFERENCES

- [1] G. R ter Haar. Therapeutic applications of ultrasound. *Prog Biophys Mol Biol.* 2007 93(1-3), pp. 111-29.
- [2] C. von zur Muhlen, D. von Elverfeldt, J.A. Moeller, R.P. Choudhury, D. Paul, C.E. Hagemeyer, M. Olschewski, A. Becker, I. Neudorfer, N. Bassler, M. Schwarz, Bode, K. Peter. Magnetic resonance imaging contrast agent targeted toward activated platelets allows in vivo detection of thrombosis and monitoring of thrombolysis. *Circulation* 118 (2008), pp. 258–267.
- [3] Z. Xu, G. Owens, D. Gordon, C. Cain, A. Ludomirsky, Non-invasive creation of an atrial septal defect by histotripsy in a canine model. *Circulation* 121 (2010), pp. 742–749.
- [4] M. Bazan-Peregrino, B. Rifai, R.C. Carlisle, J. Choi, C.D. Arvanitis, L.W. Seymour, C.C. Coussios. Cavitation-enhanced delivery of a replicating oncolytic adenovirus to tumors using focused ultrasound. *J. Controlled Release* 169 (2013), pp. 40–47.
- [6] W.J. Tyler, Y. Tufail, S. Pati. Pain: non-invasive functional neurosurgery using Ultrasound *Nature Reviews Neurology.* 6 (2010), pp. 13–14.
- [7] N. McDannold, C.M. Tempny, F.M. Fennessy, M.J. So, F.J. Rybicki, E.A. Stewart, F.A. Jolesz, K. Hynynen, Uterine leiomyomas: MR imaging-based thermometry and thermal dosimetry during focused ultrasound thermal ablation. *Radiology* 240 (2006), pp. 263–272.
- [8] S.Y. Zhang, M.X. Wan, H. Zhong, C. Xu, Z.H. Liao, H.Q. Liu, S.P. Wang. Dynamic changes of integrated backscatter, attenuation coefficient and bubble activities during high-intensity focused ultrasound (HIFU) treatment. *Ultrasound Med. Biol.* 35 (2009), pp. 1828–1844.
- [9] S.Y. Zhang, C. Li, F.Y. Zhou, M.X. Wan, S.P. Wang. Enhanced lesion-to-bubble ratio on ultrasonic Nakagami imaging for monitoring of high-intensity focused ultrasound. *J. Ultrasound Med.* 33 (2014), pp. 959–970.

- [10] K. Hynynen. MRI-guided focused ultrasound treatments. *Ultrasonics* 50 (2010), pp. 221–229.
- [11] K. B. Bader, G. Bouchoux, and C. K. Holland. *Sonothrombolysis in Therapeutic Ultrasound*, Springer (2016), pp. 339-362.
- [12] L. R. Wechsler, B. M. Demaerschalk, L. H. Schwamm, O. M. Adeoye, H. J. Audebert, C. V. Fanale, et al. Telemedicine quality and outcomes in stroke: a scientific statement for healthcare professionals from the American Heart Association/American Stroke Association. *Stroke* 48 (2017), pp. 3-25.
- [13] E. C. Jauch, J. L. Saver, H. P. Adams, A. Bruno, J. J. Connors, B. M. Demaerschalk, et al. Guidelines for the Early Management of Patients With Acute Ischemic Stroke. *A Guideline for Healthcare Professionals*. American Heart Association/American Stroke Association, vol. 44 (2013), pp. 870-947
- [14] H. Karatas, J. E. Jung, E. Lo, and K. van Leyen. Inhibiting 12/15-lipoxygenase to treat acute stroke in permanent and tPA induced thrombolysis models. *Brain Research*, 1678 (2018), pp. 123-128.
- [15] D. Tong, M. J. Reeves, A. F. Hernandez, X. Zhao, D. M. Olson, G. C. Fonarow, et al. Times From Symptom Onset to Hospital Arrival in the Get With The Guidelines–Stroke Program 2002 to 2009. *Temporal Trends and Implications* 43 (2012), pp. 1912-1917
- [16] J. L. Saver, M. Goyal, A. Van der Lugt, B. K. Menon, C. B. Majoie, D. W. Dippel, et al. Time to treatment with endovascular thrombectomy and outcomes from ischemic stroke: a meta-analysis. *JAMA* vol. 316 (2018), pp. 1279-1288.
- [17] J. L. Saver, M. Goyal, A. Bonafe, H.-C. Diener, E. I. Levy, V. M. Pereira, et al. Stent-retriever thrombectomy after intravenous t-PA vs. t-PA alone in stroke. *New England Journal of Medicine*, vol. 372 (2015), pp. 2285-2295.
- [18] W. Yang and Y. Zhou. Effect of pulse repetition frequency of high-intensity focused ultrasound on in vitro thrombolysis. *Ultrasonics sonochemistry* 35 (2017), pp. 152-160.

- [19] D. Pajek, A. Burgess, Y. Huang, and K. Hynynen. High-intensity focused ultrasound sonothrombolysis: the use of perfluorocarbon droplets to achieve clot lysis at reduced acoustic power. *Ultrasound in Medicine and Biology* 40 (2014), pp. 2151-2161.
- [20] J. T. Sutton, N. M. Ivancevich, S. R. Perrin, D. C. Vela, and C. K. Holland, "Clot retraction affects the extent of ultrasound-enhanced thrombolysis in an ex vivo porcine thrombosis model," *Ultrasound in Medicine and Biology* 39 (2013), pp. 813-824.
- [21] A. Burgess, Y. Huang, A. C. Waspe, M. Ganguly, D. E. Goertz, and K. Hynynen. High-intensity focused ultrasound (HIFU) for dissolution of clots in a rabbit model of embolic stroke. *PloS one* vol. 7 (2012), e4-2311.
- [22] C. Wright, K. Hynynen, and D. Goertz. In vitro and in vivo high intensity focused ultrasound thrombolysis. *Investigative radiology* 47, pp. 217-225.
- [23] D. Suo, S. Guo, W. Lin, X. Jiang, and Y. Jing. Thrombolysis using multi-frequency high intensity focused ultrasound at MHz range: an in vitro study. *Physics in Medicine and Biology* 60 (2015), p. 7403-7418.
- [24] A. D. Maxwell, C. A. Cain, A. P. Duryea, L. Yuan, H. S. Gurm, and Z. Xu. Noninvasive thrombolysis using pulsed ultrasound cavitation therapy–histotripsy. *Ultrasound in Medicine and Biology* 35 (2009), pp. 1982-1994.
- [25] V. A. Salgaonkar, S. Datta, C. K. Holland, and T. D. Mast. Passive cavitation imaging with ultrasound arrays. *The Journal of the Acoustical Society of America* 126 (2009), pp. 3071-3083.
- [26] J. J. Macoskey, J. R. Sukovich, T. L. Hall, C. A. Cain, and Z. Xu. Real-time acoustic-based feedback for histotripsy therapy. *The Journal of the Acoustical Society of America* 41(2017), pp. 3551-3551.
- [27] J. R. Sukovich, Z. Xu, T. L. Hall, J. J. Macoskey, and C. A. Cain. Transcranial histotripsy acoustic-backscatter localization and aberration correction for volume treatments. *The Journal of the Acoustical Society of America*, vol. 141, pp. 3490-3490, 2017.

- [28] D. Pajek and K. Hynynen. The design of a focused ultrasound transducer array for the treatment of stroke: a simulation study. *Physics in Medicine and Biology* 57 (2012), pp. 4951-4968.
- [29] G. Pinton, J.-F. Aubry, M. Fink, and M. Tanter. Numerical prediction of frequency dependent 3D maps of mechanical index thresholds in ultrasonic brain therapy. *Medical Physics* 39 (2012), pp. 455-467.
- [30] S. Pichardo, V. W. Sin, and K. Hynynen. Multi-frequency characterization of the speed of sound and attenuation coefficient for longitudinal transmission of freshly excised human skulls. *Physics in Medicine and Biology* 56 (2011), pp. 219-250.
- [31] I. Saletes, B. Gilles, V. Auboiroux, N. Bendridi, R. Salomir, and J.-C. Béra. In vitro demonstration of focused ultrasound thrombolysis using bifrequency excitation. *BioMed Research International* 2014(1): 518787
- [32] H. Cui and X. Yang. Laser enhanced high-intensity focused ultrasound thrombolysis: An in vitro study. *The Journal of the Acoustical Society of America* 133 (2013), pp. EL123-EL128.
- [33] C. Wright, K. Hynynen, and D. Goertz. An investigation of high intensity focused ultrasound thrombolysis. *AIP Conference Proceedings* (2011), pp. 246-250.
- [34] H. L. Weiss, P. Selvaraj, K. Okita, Y. Matsumoto, A. Voie, T. Hoelscher, et al. Mechanical clot damage from cavitation during sonothrombolysis. *The Journal of the Acoustical Society of America* 133 (2013), pp. 3159-3175.
- [35] B. D. Lindsey, J. D. Rojas, and P. A. Dayton. On the relationship between microbubble fragmentation, deflation and broadband superharmonic signal production. *Ultrasound in Medicine and Biology* 41 (2015), pp. 1711-1725.
- [36] G. J. Shaw, J. M. Meunier, S.-L. Huang, C. J. Lindsell, D. D. McPherson, and C. K. Holland. Ultrasound-enhanced thrombolysis with tPA-loaded echogenic liposomes. *Thrombosis research* 124 (2009), pp. 306-310.

- [37] J. Di, J. Yu, Q. Wang, S. Yao, D. Suo, Y. Ye, et al. Ultrasound-triggered noninvasive regulation of blood glucose levels using microgels integrated with insulin nanocapsules. *Nano Research* 10 (2017), pp. 1393-1402.
- [38] K. Kajiyama, K. Yoshinaka, S. Takagi, and Y. Matsumoto, "Micro-bubble enhanced HIFU," *Physics Procedia*, vol. 3, pp. 305-314, 2010.
- [39] D. J. Chung, S. H. Cho, J. M. Lee, and S.-T. Hahn, "Effect of microbubble contrast agent during high intensity focused ultrasound ablation on rabbit liver in vivo," *European Journal of Radiology*, vol. 81, pp. e519-e523, 2012.
- [40] Y. Chen, J. Jiang, Y. Zeng, X. Tian, M. Zhang, H. Wu, et al., "Effects of a microbubble ultrasound contrast agent on high-intensity focused ultrasound for uterine fibroids: a randomised controlled trial," *International Journal of Hyperthermia*, pp. 1-5, 2018.
- [41] D. Suo, Z. Jin, X. Jiang, P. A. Dayton, and Y. Jing, "Microbubble mediated dual-frequency high intensity focused ultrasound thrombolysis: An In vitro study," *Applied Physics Letters*, vol. 110, p. 023703, 2017.
- [42] D. Suo, "High Intensity Focused Ultrasound (HIFU) Based Thrombolysis Using Multiple Frequency Excitations," Ph.D. dissertation, Mechanical and Aerospace Eng., NC State Univ., Raleigh, NC, 2017.
- [43] D. Suo, B. Govind, S. Zhang, and Y. Jing, "Numerical investigation of the inertial cavitation threshold under multi-frequency ultrasound," *Ultrasonics Sonochemistry*, vol. 41, pp. 419-426, 2018.
- [44] M. Wang and Y. Zhou, "Numerical investigation of the inertial cavitation threshold by dual-frequency excitation in the fluid and tissue," *Ultrasonics Sonochemistry*, vol. 42, pp. 327-338, 2018.
- [45] Y. Zhang and S. Li, "Acoustical scattering cross section of gas bubbles under dual-frequency acoustic excitation," *Ultrasonics sonochemistry*, vol. 26, pp. 437-444, 2015.

- [46] P. A. Tatake and A. B. Pandit, "Modelling and experimental investigation into cavity dynamics and cavitation yield: influence of dual frequency ultrasound sources," *Chemical Engineering Science*, vol. 57, pp. 4987-4995, 2002.
- [47] Jason M. Meunier, Christy K. Holland, Christopher J. Lindsell, and George J. Shaw. Duty cycle dependence of ultrasound enhanced thrombolysis in a human clot model. *Ultrasound in Med. & Biol.*, 33, No. 4 (2007) pp. 576–583.
- [48] Cucai Chen, Jonathan E. Leeman, Jianjun Wang, John J. Pacella, and Flordeliza S. Villanueva. New insights into mechanisms of sonothrombolysis using ultra-high-speed imaging. *Ultrasound in Med. & Biol.*, 40, No. 1 (2014) pp. 258–262.
- [49] Mingjun Wang, Yufeng Zhou. Numerical investigation of the inertial cavitation threshold by dual frequency excitation in the fluid and tissue. *Ultrasonics - Sonochemistry* 42 (2018) 327–338.
- [50] J. Kim, W.-Y. Chang, B. D. Lindsey, P. A. Dayton, X. Dai, J. M. Stavas, et al., "Laser-generated-focused ultrasound transducers for microbubble-mediated, dual-excitation sonothrombolysis," in *Ultrasonics Symposium (IUS), 2016 IEEE International*, 2016, pp. 1-4.
- [51] Yuning Zhang, Yuning Zhang, Shengcai Li. Combination and simultaneous resonances of gas bubbles oscillating in liquids under dual-frequency acoustic excitation. *Ultrasonics Sonochemistry* 35 (2017), pp. 431-439.
- [52] Chavrier F, Chapelon J Y, Gelet A and Cathignol D. Modeling of high-intensity focused ultrasound-induced lesions in the presence of cavitation bubbles. *The Journal of the Acoustical Society of America* 108(1) (2000), pp. 432-40.
- [53] Siyuan Zhang, Zhiwei Cui, Tianqi Xu, Pan Liu, Dapeng Li, Shaoqiang Shang, Ranxiang Xu, Yujin Zong, Gang Niu, Supin Wang, Xijing He, and Mingxi Wan. Inverse effects of flowing phase-shift nanodroplets and lipid-shelled microbubbles on subsequent cavitation during focused ultrasound exposures. *Ultrasonics Sonochemistry* 34 (2017), pp. 400-409.

- [54] C.K. Holland, R.E. Apfel. An improved theory for the prediction of microcavitation thresholds. *IEEE Trans. Ultrason. Ferroelectr. Freq. Control*, 36 (2) (1989), pp. 204-208.
- [55] A. Qamar, Z.Z. Wong, J.B. Fowlkes, J.L. Bull. Dynamics of acoustic droplet vaporization in gas embolotherapy. *Appl. Phys. Lett.* 96 (2010), pp. 143702-143702.
- [56] P. Zhang, T. Porter, An in vitro study of a phase-shift nanoemulsion: a potential nucleation agent for bubble-enhanced HIFU tumor ablation. *Ultrasound Med. Biol.* 36 (2010), pp. 1856–1866.
- [57] O.D. Kripfgans, M.L. Fabiilli, P.L. Carson, J.B. Fowlkes. On the acoustic vaporization of micrometer-sized droplets, *J. Acoust. Soc. Am.* 116 (2004), pp. 272- 281.
- [58] A.H. Lo, O.D. Kripfgans, P.L. Carson, E.D. Rothman, J.B. Fowlkes, Acoustic droplet vaporization threshold: effects of pulse duration and contrast agent. *IEEE Trans. Ultrason. Ferroelectr. Freq. Control* 54 (2007), pp. 933-946.
- [59] M.L. Fabiilli, K.J. Haworth, N.H. Fakhri, O.D. Kripfgans, P.L. Carson, J.B. Fowlkes. The role of inertial cavitation in acoustic droplet vaporization, *IEEE Trans. Ultrason. Ferroelectr. Freq. Control* 56 (2009), pp. 1006-1017.
- [60] J.B. Keller and Miksis M. Bubble oscillations of large amplitude. *The Journal of the Acoustical Society of America* 68 (2) (1980), pp. 628-633.
- [61] X. Yang, C.C. Church. A model for the dynamics of gas bubbles in soft tissue. *The Journal of the Acoustical Society of America* 118 (6) (2005), pp. 3595-3606.
- [62] C.C. Church, C. Labuda, K. Nightingale. A theoretical study of inertial cavitation from acoustic radiation force impulse imaging and implications for the mechanical index. *Ultrasound in Medicine and Biology* 41 (2) (2015), pp. 472-485.
- [63] Christopher Acconcia, Ben Y. C. Leung, Anoop Manjunath, And David E. Goertz. Interactions between individual ultrasound-stimulated microbubbles and fibrin clots. *Ultrasound in Med. & Biol.*, 40, No. 9 (2014) pp. 2134–2150

APPENDICES

APPENDIX A: MATLAB code for image processing of HIFU–induced thrombolysis and control of Arduino® Braccio arm

- a. Colour images of blood clots are converted to binary images. Post–processing after cropping and adjustment of orientation (using Movavi™) entails classification of pixels as black/white with reference to RGB thresholds.

```

% 1) Program to extract frames from a movie and save individual frames to separate image
files.
% 2) Program rebuilds a new movie by recalling the saved images from disk.
% 3) Program computes the mean gray value of the color channels (if needed) and detects
the difference between a frame and the previous frame.
% 4) It uses VideoReader and Videowriter classes.

clc;
close all;           % Close all figures (except imtool figures).
imtool close all;   % Close all imtool figures.
clear;
workspace; % Make sure the workspace panel is showing.
fontSize = 22;

%%%%%%%%%%%%%%%%%%%%%%%%%%%%%%%%%%%%%%%%%%%%%%%%%%%%%%%%%%%%%%%%%%%%%%%% CHECK 1- Open the movie and get the folder %%%%%%%%%%%%%%

folder = fileparts(which('recording.mp4')); % Determine where demo folder is (works with
all versions).
movieFullFileName = fullfile(folder, 'recording.mp4'); % Pick the two movie.
%%%%%%%%%%%%%%%%%%%%%%%%%%%%%%%%%%%%%%%%%%%%%%%%%%%%%%%%%%%%%%%%%%%%%%%%

if ~exist(movieFullFileName, 'file') % Check to see that the video file exists.
    strErrorMessage = sprintf('File not found:\n%s\nYou can choose a new
one, or cancel', movieFullFileName);
    response = questdlg(strErrorMessage, 'File not found', 'OK - choose a
new movie.', 'Cancel', 'OK - choose a new movie.');
```

```

    if strcmpi(response, 'OK - choose a new movie.')
        [baseFileName, folderName, FilterIndex] =
uigetfile('*.avi');
        if ~isequal(baseFileName, 0)
            movieFullFileName =
fullfile(folderName, baseFileName);
        else
            return;
        end
    else
        return;
    end
end
try
    videoObject = VideoReader(movieFullFileName)
    numberOfFrames = videoObject.NumberOfFrames; % Determine how many
frames there are.
    vidHeight = videoObject.Height;
    vidwidth = videoObject.Width;

```

```

        numberOfFramesWritten = 0; % Prepare a
figure to show the images in the upper half of the screen.
        figure; %

screenSize = get(0, 'ScreenSize');
        set(gcf, 'units','normalized','outerposition',[0 0 1 1]); % Enlarge
figure to full screen.

        promptMessage = sprintf('Do you want to save the individual frames out
to individual disk files?'); % Ask user if they want to write the individual frames out
to disk.
        button = questdlg(promptMessage, 'Save individual frames?', 'Yes',
'No', 'Yes');
        if strcmp(button, 'Yes')
            writeToDisk = true;
            [folder, baseFileName, extensions] =
fileparts(movieFullFileName); % Extract out the various parts of the filename.
            folder = pwd;

% Make a new output subfolder for all the separately extracted movie frames to be saved
to disk
            outputFolder = sprintf('%s/Movie Frames from %s',
folder, baseFileName);

            if ~exist(outputFolder, 'dir') % Create the
folder if it doesn't exist already.
                mkdir(outputFolder);
            end

            else
                writeToDisk = false;
            end

        % Loop through the movie, writing all frames out. Each frame will be in
a separate file with unique name.
        meanGrayLevels = zeros(numberOfFrames, 1);
        meanRedLevels = zeros(numberOfFrames, 1);
        meanGreenLevels = zeros(numberOfFrames, 1);
        meanBlueLevels = zeros(numberOfFrames, 1);

        for frame = 1 : numberOfFrames
            thisFrame = read(videoObject, frame); % Extract
the frame from the movie structure.

            % Display it
            hImage = subplot(2, 2, 1);
            image(thisFrame);
            caption = sprintf('Frame %4d of %d.', frame,
numberOfFrames);

            title(caption, 'FontSize', fontSize);
            drawnow; % Force it to refresh the window.

            % Write the image array to the output file, if
requested.
            if writeToDisk

```

```

image file name.
sprintf('Frame %4.4d.png', frame);
fullfile(outputFolder, outputBaseFileName);

% Construct an output
outputBaseFileName =
outputFullFileName =

% Stamp the name and frame
number onto the image. At this point it's just going into the overlay, not actually
getting written into the pixel values.
text(5, 15,
outputBaseFileName, 'FontSize', 20);

% Extract the image with
the text "burned into" it.
frameWithText =

% framewithText.cdata is
the image with the text actually written into the pixel values. Write it out to disk.
imwrite(frameWithText.cdata, outputFullFileName, 'png');
end

% Calculate the mean gray level.
grayImage = rgb2gray(thisFrame);
meanGrayLevels(frame) = mean(grayImage(:));

% Calculate the mean R, G, and B levels.
meanRedLevels(frame) = mean(mean(thisFrame(:, :,
1)));
meanGreenLevels(frame) = mean(mean(thisFrame(:,
:, 2)));
meanBlueLevels(frame) = mean(mean(thisFrame(:, :,
3)));

%%%%%%%% CHECK 2 - Plot the binary image with threshold for clarity of blood clot. %%%%%%%%%

BW_1=im2bw(grayImage,0.3);
%%%%%%%%%%%%%%%%%%%%%%%%%%%%%%%%%%%%%%%%%%%%%%%%%%%%%%%%%%%%%%%%%%%%%%%%
n_white_with_clot(frame)=sum(BW_1(:));
n_black_with_clot(frame)=numel(BW_1)-n_white_with_clot(frame);

% CHECK 3- Plot binary image of empty tube with threshold for clarity of empty tube. %

BW_2=im2bw(grayImage,0.05);
%%%%%%%%%%%%%%%%%%%%%%%%%%%%%%%%%%%%%%%%%%%%%%%%%%%%%%%%%%%%%%%%%%%%%%%%

n_white_without_clot(frame)=sum(BW_2(:));
n_black_without_clot(frame)=numel(BW_2)-n_white_with_clot(frame);

% Percentage area removed
percent_area(frame)=((n_white_without_clot(frame)-
n_white_with_clot(frame))/n_white_without_clot(frame))*100;
end

```

```

        % Alert user that we're done.
        if writeToDisk
            finishedMessage = sprintf('Done. wrote %d frames
to folder\n"%s"', numberOfFramesWritten, outputFolder);
        else
            finishedMessage = sprintf('Done. Processed %d
frames of\n"%s"', numberOfFramesWritten, movieFullFileName);
        end
        disp(finishedMessage); % write to command window.
        uiwait(msgbox(finishedMessage)); % Also pop up a message box.

        % Exit if they didn't write any individual frames out to disk.
        if ~writeToDisk
            return;
        end

        % Ask user if they want to read the individual frames from the disk,
that they just wrote out, back into a movie and display it.
        promptMessage = sprintf('Do you want to recall the individual
frames\nback from disk into a recording?\n(This will take several seconds.)');
        button = questdlg(promptMessage, 'Recall Recording?', 'Yes', 'No',
'Yes');

        if strcmp(button, 'No')
            return;
        end

        % Create a Videowriter object to write the video out to a new,
different file.
        writerObj = Videowriter('something.avi');
        open(writerObj);

        % Read the frames back in from disk, and convert them to a movie.
Preallocate recalledMovie, which will be an array of structures. First get a cell array
with all the frames.
        allTheFrames = cell(numberOfFrames,1);
        allTheFrames(:) = {zeros(vidHeight, vidwidth, 3, 'uint8')};
        % Next get a cell array with all the colormaps.
        allTheColorMaps = cell(numberOfFrames,1);
        allTheColorMaps(:) = {zeros(256, 3)};
        % Now combine these to make the array of structures.
        recalledMovie = struct('cdata', allTheFrames, 'colormap',
allTheColorMaps)
        for frame = 1 : numberOfFrames
            % Construct an output image file name.
            outputBaseFileName = sprintf('Frame %4.4d.png',
frame);
            outputFullFileName = fullfile(outputFolder,
outputBaseFileName);

            % Read the image in from disk.
            thisFrame = imread(outputFullFileName);
            % Convert the image into a "movie frame"
            structure.
            recalledMovie(frame) = im2frame(thisFrame);

```

```

                                % Write this frame out to a new video file.
                                writeVideo(writerObj, thisFrame);

                                end
                                close(writerObj);
                                % Get rid of old image and plot.
                                delete(hImage);
                                delete(hPlot);
                                % Create new axes for our movie.
                                subplot(1, 3, 2);
                                axis off; % Turn off axes numbers.
                                title('Recording recalled from disk', 'FontSize', fontSize);
                                % Play the movie in the axes.
                                movie(recalledMovie);
                                msgbox('Done with this recording');
catch ME
                                % Some error happened if you get here.
                                strErrorMessage = sprintf('Error extracting frames
from:\n\n%s\n\nError: %s\n\n', movieFullFileName, ME.message);
                                uiwait(msgbox(strErrorMessage));
end

result='percent_area';

```

- b. MATLAB program to quantify the indentation effected by combinations of PNPs and frequency. The initial colour image of the clot is overlaid with the final image of the clot and the area of the removed clot is calculated. The code used for this analysis is bifurcated into separate steps.

```
clc; % Clear the command window.
close all; % Close all figures (except those of imtool.)
imtool close all; % Close all imtool figures.
clear; % Erase all existing variables..
workspace; % Make sure the workspace panel is showing.
format long g;
format compact;
fontSize = 24;
```

STEP 1: Read in the blood clot color image.

```
folder = 'E:\MS thesis\MS-mediated thrombolysis experiment\dip\image\Case Single\5 MPa';
baseFileName = 'dip_clot_test_s_5_b_i.png';
```

STEP 2: Get the full filename, with path prepended.

```
fullFileName = fullfile(folder, baseFileName);
if ~exist(fullFileName, 'file')

% Didn't find it there. Check the search path for it.
    fullFileName = baseFileName; % No path this time.
    if ~exist(fullFileName, 'file')
% Still didn't find it. Alert user.
        errorMessage = sprintf('Error: %s does not exist.', fullFileName);
        uiwait(warndlg(errorMessage));
        return;
    end
end
rgbImage = imread(fullFileName);
% Get the dimensions of the image. numberOfColorBands should be = 3.
[rows, columns, numberOfColorBands] = size(rgbImage);
```

STEP 3: Display the original color image of initial clot condition.

```
figure
subplot(4,1,1)
imshow(rgbImage);
title('Original Color Image of initial Clot Condition', 'FontSize', fontSize);

% Enlarge figure to full screen.
set(gcf, 'Units', 'Normalized', 'Outerposition', [0, 0, 1, 1]);
```

STEP 4: Extract the individual red, green, and blue color channels.

```
redChannel = rgbImage(:, :, 1);
greenChannel = rgbImage(:, :, 2);
blueChannel = rgbImage(:, :, 3);
```

STEP 5: Set the condition to define binary image.

```
binaryImage = redChannel < 100;

% Display the original color image.
subplot(4,1,2)
imshow(binaryImage);
axis off;
title('Initial Binary Image of initial Clot Condition', 'FontSize', fontSize);

% Clean it up.
% a. Fill holes.
binaryImage = imfill(binaryImage, 'holes');
% b. Get rid of small blobs.
binaryImage = bwareaopen(binaryImage, 5);
% c. Smoothen borders
binaryImage = imclose(binaryImage, true(5));
% d. Display the original color image.
subplot(4,1,3)
imshow(binaryImage);
axis off;
title('Cleaned Binary Image of initial Clot Condition', 'FontSize', fontSize);
```

STEP 6: Get the boundary and outline it over the original image.

```
% Display the original color image of the initial clot condition.

subplot(4,1,4)
imshow(rgbImage);
title('Outline over Original Color Image of initial Clot Condition', 'FontSize',
fontSize);
axis image; % Make sure image is not artificially stretched because of screen's aspect
ratio.
hold on;
boundaries = bwboundaries(binaryImage);
numberOfBoundaries_initial = size(boundaries, 1);
cell_x_sub_area_initial_clot=cell(1,numberOfBoundaries_initial);
cell_y_sub_area_initial_clot=cell(1,numberOfBoundaries_initial);
for j = 1 : numberOfBoundaries_initial
    thisBoundary = boundaries{j};
    cell_x_sub_area_initial_clot{j}=thisBoundary(:,2);
    cell_y_sub_area_initial_clot{j}=thisBoundary(:,1);
    plot(cell_x_sub_area_initial_clot{j},cell_y_sub_area_initial_clot{j},
'g', 'Linewidth', 2);
    % Find local x and y for each sub-area enclosed by a boundary
```

```

y_max_local(j)=max(Cell_y_sub_area_initial_clot{j});
y_min_local(j)=min(Cell_y_sub_area_initial_clot{j});
x_max_local(j)=max(Cell_x_sub_area_initial_clot{j});
x_min_local(j)=min(Cell_x_sub_area_initial_clot{j});
hold on
end

```

STEP 7: Find global maximum and minimum of the x and y coordinates of the boundaries of the initial clot condition.

```

y_max_global_initial=max(y_max_local);
y_min_global_initial=min(y_min_local);
x_max_global_initial=max(x_max_local);
x_min_global_initial=min(x_min_local);

```

STEP 8: Scale the dimensions of the initial clot to match the 10 cm clot holder's length.

```

scale=100/x_max_global_initial;

```

STEP 9: Readjust the global maximum and minimum.

```

y_max_global_initial=scale*y_max_global_initial;
y_min_global_initial=scale*y_min_global_initial;
x_max_global_initial=scale*x_max_global_initial;
x_min_global_initial=scale*x_min_global_initial;

```

STEP 10: Plot filled areas of boundaries in initial clot condition.

```

figure
for j = 1 : numberOfBoundaries_initial

    % Scale each vector in the x and y cells
    Cell_x_sub_area_initial_clot{j}=scale.*Cell_x_sub_area_initial_clot{j};
    Cell_y_sub_area_initial_clot{j}=scale.*Cell_y_sub_area_initial_clot{j};

    % Find area enclosed by each boundary

    area_of_sub_boundary_initial_clot(j)=polyarea(Cell_x_sub_area_initial_clot{j},Cell_y_sub
_area_initial_clot{j});
        plot(Cell_x_sub_area_initial_clot{j},-Cell_y_sub_area_initial_clot{j},
'r', 'Linewidth', 2);
        fill(Cell_x_sub_area_initial_clot{j},-Cell_y_sub_area_initial_clot{j}, 'r');
        xlim([x_min_global_initial,x_max_global_initial])
        ylim([-abs(y_max_global_initial)*3,abs(y_max_global_initial)*3])
        hold on
end

```

STEP 11: Find total area of initial clot condition.

```
total_area_initial_clot=sum(area_of_sub_boundary_initial_clot)
```

STEP 12: Read in the blood clot color image.

```
folder = 'E:\MS thesis\MS-mediated thrombolysis experiment\dip\image\Case Single\5 MPa';  
baseFileName = 'dip_clot_test_s_5_b_f.png';
```

STEP 13: Get the full filename, with path prepended.

```
fullFileName = fullfile(folder, baseFileName);  
if ~exist(fullFileName, 'file')  
  
    % Didn't find it there. Check the search path for it.  
    fullFileName = baseFileName; % No path this time.  
    if ~exist(fullFileName, 'file')  
    % Still didn't find it. Alert user.  
  
    errorMessage = sprintf('Error: %s does not exist.', fullFileName);  
    uiwait(warndlg(errorMessage));  
    return;  
end  
  
end  
rgbImage = imread(fullFileName);  
% Get the dimensions of the image. numberOfColorBands should be = 3.  
[rows, columns, numberOfColorBands] = size(rgbImage);
```

STEP 14: Display the original color image of final clot condition.

```
figure  
subplot(4,1,1)  
imshow(rgbImage);  
title('Original Color Image of Final Clot Condition', 'FontSize', fontSize);  
% Enlarge figure to full screen.  
set(gcf, 'Units', 'Normalized', 'Outerposition', [0, 0, 1, 1]);
```

STEP 15: Extract the individual red, green, and blue color channels.

```
redChannel = rgbImage(:, :, 1);  
greenChannel = rgbImage(:, :, 2);  
blueChannel = rgbImage(:, :, 3);
```

STEP 16: Set the condition to define binary image.

```
binaryImage = redChannel < 100;  
% Display the original color image.
```

```

subplot(4,1,2)
imshow(binaryImage);
axis off;
title('Initial Binary Image of Final Clot Condition', 'FontSize', fontSize);

% Clean it up.
% a. Fill holes.
binaryImage = imfill(binaryImage, 'holes');
% b. Get rid of small blobs.
binaryImage = bwareaopen(binaryImage, 5);
% c. Smoothen borders
binaryImage = imclose(binaryImage, true(5));
% d. Display the original color image.

subplot(4,1,3)
imshow(binaryImage);
axis off;
title('Cleaned Binary Image of Final Clot Condition', 'FontSize', fontSize);

```

STEP 17: Get the boundary and outline it over the original image.

```

% Display the original color image of the final clot condition.
subplot(4,1,4)
imshow(rgbImage);
title('Outline over Original Color Image of Final Clot Condition', 'FontSize',
fontSize);
axis image; % Make sure image is not artificially stretched because of screen's aspect
ratio.
hold on;
boundaries = bwboundaries(binaryImage);
numberOfBoundaries_final = size(boundaries, 1);
Cell_x_sub_area_final_clot=cell(1,numberOfBoundaries_final);
Cell_y_sub_area_final_clot=cell(1,numberOfBoundaries_final);

for k = 1 : numberOfBoundaries_final
    thisBoundary = boundaries{k};
    Cell_x_sub_area_final_clot{k}=thisBoundary(:,2);
    Cell_y_sub_area_final_clot{k}=thisBoundary(:,1);
    plot(Cell_x_sub_area_final_clot{k},Cell_y_sub_area_final_clot{k}, 'g',
'Linewidth', 2);
    % Find local x and y for each sub-area enclosed by a boundary
    y_max_local(k)=max(Cell_y_sub_area_final_clot{k});
    y_min_local(k)=min(Cell_y_sub_area_final_clot{k});
    x_max_local(k)=max(Cell_x_sub_area_final_clot{k});
    x_min_local(k)=min(Cell_x_sub_area_final_clot{k});
    hold on
end

```

STEP 18: Find global maximum and minimum of the x and y coordinates of the boundaries of the final clot condition

```
y_max_global_final=max(y_max_local);
y_min_global_final=min(y_min_local);
x_max_global_final=max(x_max_local);
x_min_global_final=min(x_min_local);
```

STEP 19: Scale the dimensions of the final clot to match the 10 cm clot holder's length

```
scale=100/x_max_global_final;
```

STEP 20: Readjust the global maximum and minimum

```
y_max_global_final=scale*y_max_global_final;
y_min_global_final=scale*y_min_global_final;
x_max_global_final=scale*x_max_global_final;
x_min_global_final=scale*x_min_global_final;
```

STEP 21: Plot filled areas of boundaries in final clot condition

```
figure
for k = 1 : numberOfBoundaries_final
    % Scale each vector in the x and y cells
    Cell_x_sub_area_final_clot{k}=scale.*Cell_x_sub_area_final_clot{k};
    Cell_y_sub_area_final_clot{k}=scale.*Cell_y_sub_area_final_clot{k};

    % Find area enclosed by each boundary
    area_of_sub_boundary_final_clot(k)=polyarea(Cell_x_sub_area_final_clot{k},Cell_y_sub_area_final_clot{k});
    plot(Cell_x_sub_area_final_clot{k},-Cell_y_sub_area_final_clot{k}, 'r', 'Linewidth',
    2);
    fill(Cell_x_sub_area_final_clot{k},-Cell_y_sub_area_final_clot{k}, 'r');
    xlim([x_min_global_final,x_max_global_final])
    ylim([-abs(y_max_global_final)*3,abs(y_max_global_final)*3])
    hold on
end
```

STEP 22: Find total area of final clot condition

```
total_area_final_clot=sum(area_of_sub_boundary_final_clot)
```

STEP 23: Plot initial and final clots' outlines on the same figure

```
figure
for j = 1 : numberOfBoundaries_initial
    plot(Cell_x_sub_area_initial_clot{j},-Cell_y_sub_area_initial_clot{j}, 'b', 'Linewidth',
    1);
```

```

end
hold on
for k = 1 : numberOfBoundaries_final
plot(Cell_x_sub_area_final_clot{k},-Cell_y_sub_area_final_clot{k}, 'r', 'Linewidth', 1);
end

grid on
legend('Original clot condition','Final clot condition')
title('Original and final clot condition outline')
xlim([x_min_global_initial,x_max_global_initial])
ylim([-abs(y_max_global_initial)*3,abs(y_max_global_initial)*3])
xlabel('Movement along x-axis(mm)')

% Enter left and right limits of clot under investigation
y_n=1; % Initially run the program

% Input left and right limits for shortened x and y vectors for removed clot
visualization
while y_n==1

prompt_input_left = 'Enter left limit of particular segment of clot (in mm): '; % asks
for left limit for shortened clot
input_left = input(prompt_input_left);

prompt_input_right = 'Enter right limit of particular segment of clot (in mm): '; % asks
for left limit for shortened clot
input_right = input(prompt_input_right);

```

STEP 24: Finding initial shortened clot area

```

for j = 1 : numberOfBoundaries_initial

% Define unaltered x and y vectors representing each boundary in the cell
Cell_x_sub_area_initial_clot_shortened{j}=Cell_x_sub_area_initial_clot{j};
Cell_y_sub_area_initial_clot_shortened{j}=Cell_y_sub_area_initial_clot{j};

% Find index for elements left of the input left limit and delete these elements
index_left_initial = find(Cell_x_sub_area_initial_clot_shortened{j} < input_left);
% y-values for x less than this index (x-distance) will be deleted
Cell_x_sub_area_initial_clot_shortened{j}(index_left_initial)=[];
Cell_y_sub_area_initial_clot_shortened{j}(index_left_initial)=[];

% Find index for elements right of the input left limit and delete these elements
index_right_initial = find(Cell_x_sub_area_initial_clot_shortened{j} > input_right);
% y-values for x less than this index (x-distance) will be deleted
Cell_x_sub_area_initial_clot_shortened{j}(index_right_initial)=[];
Cell_y_sub_area_initial_clot_shortened{j}(index_right_initial)=[];

area_of_sub_boundary_initial_shortened_clot(j)=polyarea(Cell_x_sub_area_initial_clot_sho
rtened{j},Cell_y_sub_area_initial_clot_shortened{j});
end

```

```
sum_of_area_of_sub_boundary_initial_shortened_cлот=sum(area_of_sub_boundary_initial_shortened_cлот)
```

STEP 25: Finding final shortened clot area

```
for k = 1 : numberOfBoundaries_final

    % Define unaltered x and y vectors representing each boundary in the cell
    Cell_x_sub_area_final_cлот_shortened{k}=Cell_x_sub_area_final_cлот{k};
    Cell_y_sub_area_final_cлот_shortened{k}=Cell_y_sub_area_final_cлот{k};

    % Find index for elements left of the input left limit and delete these elements
    index_left_final = find(Cell_x_sub_area_final_cлот_shortened{k} < input_left);
    % y-values for x less than this index (x-distance) will be deleted
    Cell_x_sub_area_final_cлот_shortened{k}(index_left_final)=[];
    Cell_y_sub_area_final_cлот_shortened{k}(index_left_final)=[];

    % Find index for elements right of the input left limit and delete these elements
    index_right_final = find(Cell_x_sub_area_final_cлот_shortened{k} > input_right);
    % y-values for x less than this index (x-distance) will be deleted
    Cell_x_sub_area_final_cлот_shortened{k}(index_right_final)=[];
    Cell_y_sub_area_final_cлот_shortened{k}(index_right_final)=[];

    area_of_sub_boundary_final_shortened_cлот(k)=polyarea(Cell_x_sub_area_final_cлот_shortened{k},Cell_y_sub_area_final_cлот_shortened{k});
end

sum_of_area_of_sub_boundary_final_shortened_cлот=sum(area_of_sub_boundary_final_shortened_cлот)
```

STEP 26: Calculation of initial, final and removed areas of initial, final and shortened final clot

```
Area_of_removed_cлот_in_short_segment=
sum_of_area_of_sub_boundary_initial_shortened_cлот -
sum_of_area_of_sub_boundary_final_shortened_cлот;
```

```
figure
% Plot initial clot condition
subplot(4,1,1)
for j = 1 : numberOfBoundaries_initial

    plot(Cell_x_sub_area_initial_cлот{j},-Cell_y_sub_area_initial_cлот{j},
'r', 'Linewidth', 2);
    fill(Cell_x_sub_area_initial_cлот{j},-Cell_y_sub_area_initial_cлот{j}, 'r');
    xlim([x_min_global_initial,x_max_global_initial])
    grid on
    hold on
end
title('Initial clot condition')

% Plot final clot condition
subplot(4,1,2)
```

```

for k = 1 : numberOfBoundaries_final
    plot(Cell_x_sub_area_final_clot{k},-Cell_y_sub_area_final_clot{k}, 'r',
'Linewidth', 2);
    fill(Cell_x_sub_area_final_clot{k},-Cell_y_sub_area_final_clot{k}, 'r');
    xlim([x_min_global_initial,x_max_global_initial])
    grid on
    hold on
end
title('Final clot condition')

% Plot initial and final clot conditions on same plot
subplot (4,1,3)
for j = 1 : numberOfBoundaries_initial
    plot(Cell_x_sub_area_initial_clot{j},-Cell_y_sub_area_initial_clot{j},
'w', 'Linewidth', 2);
    fill(Cell_x_sub_area_initial_clot{j},-Cell_y_sub_area_initial_clot{j}, [1 0.5 0.3]);
    xlim([x_min_global_initial,x_max_global_initial])
    grid on
    hold on
end

for k = 1 : numberOfBoundaries_final
    plot(Cell_x_sub_area_final_clot{k},-Cell_y_sub_area_final_clot{k}, 'r',
'Linewidth', 2);
    fill(Cell_x_sub_area_final_clot{k},-Cell_y_sub_area_final_clot{k}, 'w');
    xlim([x_min_global_initial,x_max_global_initial])
    grid on
    hold on
end
title('Total clot removed')

% Plot shortened clot condition
subplot (4,1,4)
for j = 1 : numberOfBoundaries_initial
    plot(Cell_x_sub_area_initial_clot_shortened{j},-
Cell_y_sub_area_initial_clot_shortened{j}, 'w', 'Linewidth', 2);
    fill(Cell_x_sub_area_initial_clot_shortened{j},-
Cell_y_sub_area_initial_clot_shortened{j}, [1 0.5 0.3]);
    xlim([x_min_global_initial,x_max_global_initial])
    grid on
    hold on
end

for k = 1 : numberOfBoundaries_final
    plot(Cell_x_sub_area_final_clot_shortened{k},-
Cell_y_sub_area_final_clot_shortened{k}, 'r', 'Linewidth', 2);
    fill(Cell_x_sub_area_final_clot_shortened{k},-
Cell_y_sub_area_final_clot_shortened{k}, 'w');
    xlim([x_min_global_initial,x_max_global_initial])
    grid on
    hold on
end
title('Clot removed in the queried subsection')

```

```
end
```

- c. The movement of the 'Braccio' arm is realized by the integration of an Arduino 'Uno' microcontroller with six servo motors. Joint angles are relayed to the microcontroller via USB connection and the arm is actuated to assume the desired orientation. The following MATLAB program illustrates the use of just two degrees of freedom (elbow and shoulder joints), while in practice all six degrees of freedom may be utilized for greater mobility.

```
% This program assists in the visualization of workspace movement of the
% Braccio arm and trains the arm to achieve joint angle combinations for
% permutations of X-Y-Z co-ordinates.

clear all
clc

% General 3-D movement for swivel mode/ normal mode

l1 = 1304.2;          % length of first movable arm in 'decimm'
l2 = 1281.8;          % length of second movable arm in 'decimm'
l3 = 1692.2;          % length of third movable arm in 'decimm'
focuslength=300;    % length of focus in 'decimm'
l3=l3+focuslength;  % effective length

correctionb= 4;      % Current correction in base angle
correction1= -1;     % Current correction in theta_1
correction2= -7;     % Current correction in theta_2
correction3= -2;     % Current correction in theta_3

thetab = [-0.26:0.005:0.26]; % all possible base angle values from -15 to 15 degrees
theta1 = [0:0.04:1.22];      % all possible theta1 (shoulder) values from 0 to 75
degrees
theta2 = [-1.22:0.04:1.22]; % all possible theta2 (elbow) values from 0 to 75 degrees
theta3 = [-1.22:0.04:1.22]; % all possible theta3 (wrist) values from -75 to 75
degrees

% 3-D movement

for i=1:length(thetab)
    for j=1:length(theta1)
        for k=1:length(theta2)
            for l=1:length(theta3)
                new_3DX(i,j,k,l) = l1*cos(theta1(j)) + l2*cos(theta1(j)+theta2(k)) +
                (l3)*cos(theta1(j)+theta2(k)+theta3(l)) ; % compute x coordinates
                new_3DY(i,j,k,l) = cos(thetab(i)).*(l1*sin(theta1(j)) +
                l2*sin(theta1(j)+theta2(k)) + (l3)*sin(theta1(j)+theta2(k)+theta3(l))) ; % compute y
                coordinates
                new_3DZ(i,j,k,l) = sin(thetab(i)).*(l1*sin(theta1(j)) +
                l2*sin(theta1(j)+theta2(k)) + (l3)*sin(theta1(j)+theta2(k)+theta3(l))) ; % compute z
                coordinates
            end
        end
    end
end
```

```

end
end

% 2-D movement

for j=1:length(theta1)
    for k=1:length(theta2)
        for l=1:length(theta3)
            new_2DX(i,j,k,l) = l1*cos(theta1(j)) + l2*cos(theta1(j)+theta2(k)) +
(13)*cos(theta1(j)+theta2(k)+theta3(l)) ; % compute x coordinates
            new_2DY(i,j,k,l) = (l1*sin(theta1(j)) + l2*sin(theta1(j)+theta2(k)) +
(13)*sin(theta1(j)+theta2(k)+theta3(l))) ; % compute y coordinates

        end
    end
end

figure(1)
plot(new_2DX(:),new_2DY(:),'r. ');
xlabel('X','fontsize',10)
ylabel('Y','fontsize',10)
title('Sample 2-D movement generated for all \theta_2, \theta_3 and \theta_4
combinations using forward kinematics','fontsize',10)

figure(2)

plot3(new_3DX(:),new_3DY(:),new_3DZ(:),'r. ');

xlabel('X','fontsize',10)
ylabel('Y','fontsize',10)
zlabel('Z','fontsize',10)
title('3-D movement generated for all \theta_1, \theta_2, \theta_3 and \theta_4
combinations using forward kinematics','fontsize',10)

new_3DX=floor(new_3DX./1)*1; % round off to nearest 'decimm'
new_3DY=floor(new_3DY./1)*1; % round off to nearest 'decimm'
new_3DZ=floor(new_3DZ./1)*1; % round off to nearest 'decimm'

```

STEP 1: The connection with the Arduino micro-controller is now opened.

```

arduino=serial('COM9','BaudRate',9600); % create serial communication object on port
COM4

fopen(arduino); % initiate arduino communication
flag=1;
prompt='Enter mode: 1 to enter co-ordinates, 2 to manually enter angles ';
str=input(prompt,'s');

```

STEP 2: Enters a mode of manual entry of angles if option 2 is selected.

```
if str=='2'

while (flag==1)
promptb = 'Enter theta_b: ';
thetab_string=num2str(input(promptb)+correctionb);

prompt1 = 'Enter theta_1: ';
theta1_string=num2str((90-(input(prompt1))+correction1));

prompt2 = 'Enter theta_2: ';
theta2_string=num2str((90-(input(prompt2))+correction2));

prompt3 = 'Enter theta_3: ';
theta3_string=num2str((90-input(prompt3)+correction3));

% Combines the angles in a string to be input to arduino

string_for_arduino= [thetab_string ',' theta1_string ',' theta2_string ','
theta3_string];

fprintf(arduino,'%s',string_for_arduino); % send answer variable content to arduino
end
end
```

STEP 3: Enters a mode of manual entry of coordinates if option 1 is selected.

```
if str=='1' % Enter coordinates

while (flag==1)

prompt_x = 'Enter x-coordinate in mm (to one decimal place): '; % asks for x
coordinate in mm
str_x = input(prompt_x);
str_x=str_x*10;

prompt_y = 'Enter y-coordinate in mm (to one decimal place): '; % asks for y
coordinate in mm
str_y = input(prompt_y);
str_y=str_y*10;

prompt_z = 'Enter z-coordinate in mm (to one decimal place): '; % asks for z
coordinate in mm
str_z = input(prompt_z);
str_z=str_z*10;

count=0;

% Enters this mode if entered coordinates cannot be found - most probability
```

```

if count==0
disp("These coordinates cannot be directly reached by the arm. However, the arm will
move to the following nearest point:");

% Matrix of distance from the entered coordinates is calculated

diff_x=abs(str_x-new_3DX);
diff_y=abs(str_y-new_3DY);
diff_z=abs(str_z-new_3DZ);

for i=1:length(thetab)
    for j=1:length(theta1)
        for k=1:length(theta2)
            for l=1:length(theta3)

del_xyz(i,j,k,l)=sqrt((diff_x(i,j,k,l).^2)+(diff_y(i,j,k,l).^2)+(diff_z(i,j,k,l).^2));

                end
            end
        end
    end

    min_del=min(del_xyz); % The point with the least distance is
selected
    [M,I] = min(del_xyz(:));
    [I, J,K,L] = ind2sub(size(del_xyz),I);
    new_x=new_3DX(I,J,K,L)/10;
    new_y=new_3DY(I,J,K,L)/10;
    new_z=new_3DZ(I,J,K,L)/10;
    new_point=[new_x,new_y,new_z];
    disp(new_point);
    new_angles=[thetab(I),theta1(J),theta2(K),theta3(L)];
    new_angles_round=round(new_angles*180/pi);

disp("The corresponding thetab, theta1, theta2 and theta3 to nearest integer are");
disp(new_angles_round);

end
str_thetab=num2str(new_angles_round(1)+correctionb);
str_theta1=num2str((90-new_angles_round(2)+correction1));
str_theta2=num2str((90-new_angles_round(3)+correction2));
str_theta3=num2str((90-new_angles_round(4)+correction3));

string_for_arduino= [str_thetab ',' str_theta1 ',' str_theta2 ',' str_theta3];

fprintf(arduino,'%s',string_for_arduino); % send answer variable content to arduino
end
end

fclose(arduino); % end communication with arduino
delete(instrfind({'Port'},{'COM9'}));

```

APPENDIX B: Representative images used in post-processing for quantification of site-specific clot indentation size for DFFU (1.45 MHz +1.5 MHz) (a-e) and SFFU (1.5 MHz) (f-j)



(a)



(b)



(c)



(d)



(e)



(f)



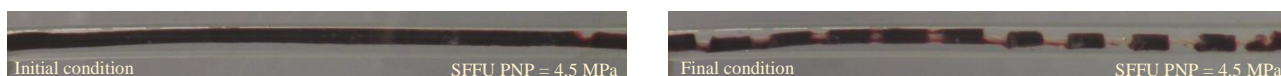
(g)



(h)



(i)



(j)